Wu et al. *Zool. Res.* 2025, 46(1): 122−138
https://doi.org/10.24272/j.issn.2095-8137.2024.211
https://cstr.cn/32248.14.zr.2024.211

ZR | Zoological Research

Article Open Access

Transcription coactivator YAP1 promotes CCND1/CDK6 expression, stimulating cell proliferation in cloned cattle placentas

Shan-Shan Wu[1,2,#], Xiao-Yu Zhao[1,2,#], Lei Yang[1,2], Chao Hai[1,2], Di Wu[1,2], Xue-Fei Liu[1,2], Li-Shuang Song[1,2], Chun-Ling Bai[1,2], Guang-Hua Su[1,2,*], Guang-Peng Li[1,2,*]

[1] *State Key Laboratory of Reproductive Regulation and Breeding of Grassland Livestock (R2BGL)*, *Inner Mongolia University*, *Hohhot*, *Inner Mongolia* 010070, *China*

[2] *College of Life Sciences*, *Inner Mongolia University*, *Hohhot*, *Inner Mongolia* 010070, *China*

ABSTRACT

Somatic cell nuclear transfer (SCNT) has been successfully employed across various mammalian species, yet cloned animals consistently exhibit low pregnancy rates, primarily due to placental abnormalities such as hyperplasia and hypertrophy. This study investigated the involvement of the Hippo signaling pathway in aberrant placental development in SCNT-induced bovine pregnancies. SCNT-derived cattle exhibited placental hypertrophy, including enlarged abdominal circumference and altered placental cotyledon morphology. RNA sequencing analysis indicated significant dysregulation of Hippo signaling pathway genes in SCNT placentas. Co-expression of YAP1 and CCND1 was observed in cloned blastocysts, placental tissues, and bovine placental mesenchymal stem cells (bPMSCs). Manipulation of YAP1 expression demonstrated the capacity to regulate bPMSC proliferation. Experimental assays confirmed the direct binding of YAP1 to CCND1, which subsequently promoted CCND1 expression in bPMSCs. Furthermore, inhibition of CDK6, a downstream target of CCND1, attenuated SCNT bPMSC proliferation. This study identified YAP1 as a key regulatory component within the Hippo signaling pathway that drives placental hyperplasia in cloned cattle through up-regulation of CCND1-CDK6 expression, facilitating cell cycle progression. These findings offer potential avenues for enhancing cloning efficiency, with implications for evolutionary biology and the conservation of valuable germplasm resources.

Keywords: Somatic cell nuclear transfer; Cloned cattle; Placental hypertrophy; Cell proliferation; CCND1-CDK6; YAP1

INTRODUCTION

Somatic cell nuclear transfer (SCNT) is a powerful technique in animal biotechnology, enabling the rapid duplication and enhancement of desirable traits in livestock, thus making invaluable contributions to animal breeding programs (Matoba & Zhang, 2018). SCNT technology also has broad applications in the fields of transgenic animal reproduction, evolution, germplasm preservation, endangered species protection, organ transplantation, and fundamental biological research (Matoba & Zhang, 2018; Oback, 2008; Ogura et al., 2013; Vajta, 2007).

Despite its potential, SCNT-based cloning in animals continues to show low efficiency, with birth success rates remaining limited (Yang et al., 2007). For instance, survival rates for SCNT-derived sheep, cattle, pigs, and mice have been reported to range from 0.5% to 18% (Tsunoda & Kato, 2002). A nine-year survey in Japan observed an average success rate of 4.3% in cloned cattle (Watanabe & Nagai, 2011), while a recent 2022 review confirmed critically low success rates across species, fluctuating between 0.1% and 5% (Samiec, 2022).

The low efficiency in generating SCNT-derived progeny is predominantly linked to the limited capacity of nuclear donor

Received: 08 September 2024; Accepted: 22 October 2024; Online: 23 October 2024

Foundation items: This study was supported by the National Natural Science Foundation of China (32060755), Natural Science Foundation of Inner Mongolia (2024MS03001), Inner Mongolia Autonomous Region Open Competition Projects (2022JBGS0018), Program for Young Talents of Science and Technology in Universities of Inner Mongolia Autonomous Region (NJYT23090), Inner Mongolia Autonomous Region Science and Technology Leading Team (2022LJRC0006), Inner Mongolia Autonomous Region Science and Technology Major Project (2021ZD0009), Major Agricultural Science and Technology Project of the Ministry of Agriculture and Rural Affairs (NK2022130203), Central Government Guides Local Science and Technology Development Funds (2022ZY0212), Inner Mongolia Autonomous Region High-level Talent Support Program, and Inner Mongolia University Chief Scientist Program

[#]Authors contributed equally to this work

*Corresponding authors, E-mail: guanghuasu@imu.edu.cn; gpengli@imu.edu.cn

cells (NDCs) to undergo epigenetic reprogramming of their transcriptomic and proteomic profiles within nuclear-transferred embryos. The efficiency of this reprogramming process is highly dependent on the histological origin of the NDCs, their levels of stemness and differentiation, and the synchronization of their cell cycle to the G0/G1 phases (Gorczyca et al., 2021; Huang et al., 2023; Min et al., 2015; Samiec & Skrzyszowska, 2010). Additionally, incompatibilities in meiotic, epigenomic, and cytoplasmic maturation processes within *in vitro* cultured nuclear recipient oocytes (NROs) often lead to aberrant activation of the embryo-specific developmental program in nuclear-transferred oocytes (Canel et al., 2010; Gorczyca et al., 2022; Ross et al., 2009; Skrzyszowska et al., 2008). Equally significant are issues related to asynchronous or non-synergistic interactions among inter-genomic, inter-epigenomic, inter-transcriptomic, and inter-proteomic pathways between nuclear and mitochondrial compartments, which derive from both NDCs and enucleated NROs used to propagate SCNT-derived embryos (Jiao et al., 2007; Samie & Skrzyszowska, 2005; Yan et al., 2010). Cloned embryos, fetuses, and offspring are susceptible to various developmental abnormalities throughout gestation, including large offspring syndrome, early embryonic and fetal losses, elevated perinatal mortality, prolonged gestation, increased abdominal girth, excessive amniotic fluid, and enlarged placenta (Hwang et al., 2015; Svarcova et al., 2007).

Overcoming the hurdles of low efficiency and abnormal development in cloned mammals has become a central focus in SCNT research (Samiec, 2022; Sangalli et al., 2023). Placental abnormalities are major contributors to the low success rates of cloned pregnancies (Chavatte-Palmer et al., 2006), impairing nutrient transport and fetal development (Whitworth & Prather, 2010). During the blastocyst stage, embryonic differentiation leads to the formation of the inner cell mass (ICM) and trophectoderm (TE), with the latter developing into the placenta. The placenta plays a crucial role in nutrient transport and hormone synthesis, directly influencing fetal growth and development (Tanaka et al., 2001).

Placental enlargement in SCNT animals is attributed to multiple factors, including dysregulated hormone secretion, abnormal DNA methylation and RNA expression (Arnold et al., 2008; Malin et al., 2022), and most notably, abnormal chromatin histone modifications and imprinting gene expression (Ogura et al., 2021; Ticiani et al., 2020). Wang et al. (2020) found that histone H3 lysine 27 trimethylation (H3K27me3) is associated with the up-regulation of imprint coding genes, such as Scm-like with four MBT domains 2 (*Sfmbt2*), GRB2-associated binding protein 1 (*Gab1*), and SPARC-related modular calcium binding (*Smoc1*), in cloned mouse placentas. Similarly, Arnold et al. (2017) reported increased levels of histone H3 lysine 4 dimethylation (H3K4me2) in the placental tissues of cloned cattle fetuses at day 60 of pregnancy, with relatively lower, though not significantly, levels of H3K9me2. Zhou et al. (2020) demonstrated that H3K4me3 loss during embryonic development enhances the growth of cloned cattle embryos. Studies have also identified aberrant hormone expression, including progesterone and placental lactogens, as a crucial factor contributing to placental enlargement in cloned placentas (Bajoria et al., 2002; Hill, 2014). Currently, however, research on effective repair strategies for placental abnormalities in cloned animals remains scarce. Most studies have focused on genetic interventions aimed at rescuing abnormal epigenetic reprogramming, specifically through the modulation of DNA methylation and histone modifications, alongside the targeted overexpression or suppression of genes involved in embryonic development (Srirattana et al., 2022). Our earlier studies identified abnormal expression of circular RNAs (circRNAs), long non-coding RNAs (lncRNAs), microRNAs (miRNAs), and competing endogenous RNAs (CeRNAs) in SCNT-derived bovine placentas, particularly those regulated by the DNA methylation hydroxylase Tet methylcytosine dioxygenase 1 (TET1), influenced by BTA-miR-1298 and lncRNAMSTRG.119672 (Gao et al., 2019; Su et al., 2019).

Mesenchymal stem cells (MSCs) exhibit pluripotency and paracrine signaling capabilities, allowing differentiation into cell types closely related to placental formation. Placental MSCs (PMSCs), in particular, contribute to early placental angiogenesis by differentiating into cells that form vascular structures (Boss et al., 2018). PMSCs further support placental function through paracrine interaction with other constituent placental cells, improving angiogenesis, enhancing uterine spiral artery remodeling, and regulating uteroplacental immune dynamics (Liu et al., 2021; Magatti et al., 2019; Wu et al., 2020). Successful placental growth requires a precise balance among cell proliferation, differentiation, and apoptosis (Peter, 2013). Placental formation and development are regulated by a variety of signaling pathways and growth factors, some of which may induce abnormal or accelerated cell proliferation, although comprehensive research on this topic remains limited.

Several cell signaling pathways, including the Hippo/Yap1, PI3K/Akt, Notch, and Wnt/β-catenin signaling pathways, are key regulators of organ size and placental development (Camargo et al., 2007; Dong et al., 2007). Among these, the Hippo signaling pathway plays a central role in promoting cell proliferation and suppressing cell differentiation through positive regulation of the Yes1-associated transcriptional regulator (*Yap1*), an essential factor in organ size control (Heallen et al., 2011; Moon et al., 2018). In human placental tissues, the Hippo pathway also plays a crucial role in placental development by promoting cell proliferation and maintaining stemness (Meinhardt et al., 2020). CCND1 and CDK6 act as important regulators of cellular proliferation, particularly during the G1 phase of the cell cycle, facilitating the G1-S transition that drives cell division (Li et al., 2018a). In SCNT cattle, placental overgrowth-characterized by increased cell numbers, hypertrophy, and stromal expansion-may contribute to placental enlargement, although further studies are needed to determine the involvement of the Hippo pathway in this condition.

Evolution has shaped the role of the Hippo signaling pathway in placental development, and disruptions in this pathway can lead to the development of abnormalities. Exploring these regulatory mechanisms can provide insights into both evolutionary biology and developmental processes. Furthermore, the preservation and utilization of germplasm resources are essential for maintaining genetic diversity and adaptability in agricultural species. Effective advancements in SCNT technology can support the conservation and propagation of valuable genetic traits, ensuring species resilience under changing environments. This study is important for revealing the regulatory mechanisms underlying placental gigantism in SCNT-derived animals and for

improving cloning efficiency, contributing to the advancement of cloned animal production.

MATERIALS AND METHODS

Ethics statement

All animals used in the study were treated following the Council of China Animal Welfare guidelines. All protocols were approved by the Institutional Animal Care and Use Committee at Inner Mongolia University (approval number: IMU-CATTLE-2022-063).

Analysis of gestational indicators in recipient cows of cloned cattle and determination of postpartum placental phenotypes

All cattle used in this study were raised under consistent conditions at the NeiDaShengMu High-Tech Livestock Farming Company facility in Hohhot city and Heling District. The cloned cattle group was derived from donor ear-tip fibroblasts obtained from a high-quality 2-year-old bull, while the control (CON) group consisted of cattle naturally impregnated through artificial insemination. Both groups included pregnant cows aged 18–22 months, all fed the same forage and maintained under the same conditions. In the CON group, gestation period calculations began from the breeding date immediately following estrus, with the birth date of the calf marking the end of gestation (gestation period = calf birth date − cow breeding date). In the SCNT group, gestation period calculations began from the estrus date. Cloned embryos were transferred into recipient uteruses 7 days post-estrus (gestation period = calf birth date − cow estrus date). By using estrus as the starting point in both groups, the initial reference time remained consistent across comparisons. After delivery, placental tissue samples from both the CON and SCNT groups were collected for phenotypic assessment. Placental parameters were recorded, including number, length, and width of cotyledons, as well as birth weight of the cloned calves. All data were subsequently subjected to statistical analysis.

RNA sequencing (RNA-seq) of placental tissue

Placental tissue samples were obtained from three CON cattle and three SCNT cattle. Total RNA was extracted, followed by RNA-seq library construction. Sequencing was performed on the Illumina NovaSeq 6000 Sequencing Platform (USA). The RNA-seq data were subjected to quality control using the Fastx-toolkit (v.0.014) and Fastp (v.0.19.5, http://github.com/OpenGene/fastp) software (reference gene source: *Bos taurus*; reference genome version: ARS-UCD1.2). Read mapping to the genome was performed using Bowtie alignment software. Differential expression analysis was conducted using DESeq2 (http://bioconductor.org/packages/stats/bioc/DESeq2/), applying a filtering threshold of $|\log_2 FC| \geq 1$ and $P<0.05$ to identify differentially expressed genes (DEGs). Gene Ontology (GO, https://geneontology.org/) and Kyoto Encyclopedia of Genes and Genomes (KEGG, https://www.genome.jp/kegg/) pathway analyses were performed using the DAVID database.

Isolation, cultivation, and differentiation analysis of bovine PMSCs (bPMSCs)

The isolation and culture protocols for bPMSCs followed previous research (Lankford et al., 2017). Briefly, placental chorionic membrane tissue was washed in phosphate-buffered saline (PBS, Gibco, USA) containing 2% penicillin-streptomycin (Gibco, USA), dissected into small fragments, and digested with an enzyme solution comprising 0.25% trypsin (Gibco, USA) and 1% Type IV collagenase (Gibco, USA) at a 1:1 ratio. Tissue digestion was carried out in three cycles at 37°C, each lasting 30 min. The digested cell suspension was then seeded in Dulbecco's Modified Eagle Medium/Nutrient Mixture F-12 (DMEM-F12, Gibco, USA) enriched with 20% fetal bovine serum (FBS, Gibco, USA) and 1% penicillin-streptomycin and incubated at 37°C in a humidified 5% CO_2 environment. Cells were subcultured upon reaching 95% confluence, typically at a 1:3 ratio, or cryopreserved for future use. Differentiation assays for MSCs involved the use of adipogenic induction culture A medium (DMEM-F12, 10% FBS, 1% glutamine (Gibco, USA), 0.2% insulin (Sigma, USA), 0.1% dexamethasone (Sigma, USA), 0.1% IBMX (Sigma, USA), and 0.1% rosiglitazone (Sigma, USA)) and adipogenic induction culture B medium (DMEM-F12, 10% FBS, 1% glutamine, and 0.2% insulin), with alternate treatments over 3–5 cycles (12–20 days) to induce adipogenic differentiation. The cells were stained with Oil Red O staining solution and imaged under a microscope (ZEISS, Germany). For osteogenic differentiation, bPMSCs were cultured in osteogenic induction culture medium (DMEM-F12, 15% FBS, 1% 1 mol/L β-glycerophosphate (Gibco, USA), 2% dexamethasone (Gibco, USA), and 2% ascorbate (Gibco, USA)) for 12–28 days, with differentiation evaluated using Alizarin Red S staining under microscopy. In this study, Yap1 expression was inhibited in CON and SCNT bPMSCs by the addition of 100 nmol/L verteporfin (CL318952, MCE, USA) during culture. Additionally, SCNT bPMSCs were further validated by treatment with the CDK4/CDK6 inhibitor BSJ-03-204 (effective inhibitory concentration of 26.9 nmol/L for CDK4/CCND1 and 10.4 nmol/L for CDK6/CCND1) (HY-136250, MCE, USA).

Construction of lentiviral vectors for YAP1 overexpression/knockdown and establishment of stable cell lines

To construct the YAP1 overexpression vector, YAP1 DNA was inserted into the PCDH-CMV-EF1-T2A-Puro vector. Four short hairpin RNAs (shRNAs) targeting the YAP1 gene were designed using the Invitrogen and Gene Link interference fragment design platform (Dalian Baio Biological, China) (Supplementary Table S1). These shRNAs were converted into double-stranded DNA and inserted into the PLKO.1-CopGFE-Puro vector to create the YAP1 knockdown vector. The resulting vectors were subsequently transformed into Stbl3 *Escherichia coli* competent cells, sequenced for verification, and subsequently used for YAP1 overexpression and knockdown experiments.

For lentivirus production, Lipofectamine 2000 (Invitrogen, 11668019, USA) was used to co-transfect 293T cells with the auxiliary packaging plasmids psPAX2 and pMD2G, along with the lentiviral shuttle plasmids PCDH-CMV-EF1-T2A-Puro-YAP1 or PLKO.1-CopGFP-Puro-shYAP1, at a shuttle plasmid-to-pMD2G:psPAX2 ratio of 5:2:3. After 6 h of transfection, the culture medium was replaced with fresh complete medium (DMEM-F12 supplemented with 10% FBS and 1% penicillin-streptomycin). The cells were cultured at 37°C with 5% CO_2 under high humidity for 24 h and 48 h, after which cell supernatants enriched with YAP1-overexpressing/knockdown lentivirus particles were collected. The lentivirus was concentrated using the PEG-8000 method, and the resulting

lentiviral pellet was dissolved in an appropriate amount of PBS and aliquoted for storage at −80°C. For bPMSC infection, the concentrated viral suspension was applied to the cells. After 48 h of transfection, fluorescence was observed under an inverted fluorescence microscope (ZEISS, Germany).

Preparation of *in vitro* fertilization (IVF) and SCNT embryos

IVF embryos were generated following the procedures outlined in our previous study (Su et al., 2021a). Cumulus-oocyte complexes (COCs) were collected from ovarian follicles, measuring 3–8 mm in diameter, obtained from a slaughterhouse. *In vitro* maturation (IVM) of the oocytes was achieved using an IVM medium (M199 Gibco USA, 10 mmol/L HEPES sigma USA, 10% FBS, 0.01 μg/mL FSH sigma USA, 1 μg/mL LH sigma USA, and 0.01 μg/mL E2 sigma USA). For fertilization, frozen-thawed semen from verified fertile bulls was used. Post-fertilization, the embryos were washed and cultured in BO-IVC medium (71005, IVF Bioscience, UK) at 38.5°C under 5% CO_2 saturation and high humidity.

SCNT was performed as described in our previous study (Su et al., 2021b). Briefly, donor fibroblasts were introduced into the perivitelline space of enucleated oocytes. Successfully reconstructed embryos underwent electrofusion 30 min later and were subsequently cultured in SOF medium at 38.5°C under 5% CO_2 saturation and high humidity for 30 min. All fused embryos were activated in 5 μmol/L ionomycin (sigma USA) for 5 min, followed by incubation in 10 μg/mL cycloheximide (Sigma, USA) for 5 h. The embryos were then transferred to SOF development medium, covered with mineral oil, and cultured at 38.5°C under 5% CO_2 saturation and high humidity. After 48 h, the cells were co-cultured on a granulosa cell layer to support development to the blastocyst stage.

Reverse transcription-quantitative real-time polymerase chain reaction (RT-qPCR)

mRNA from blastocyst-stage embryos was extracted using an Arcturus PicoPure RNA Isolation Kit (65032D, Thermo, USA) following the provided instructions. The isolated mRNA was subsequently reverse-transcribed into cDNA using a PrimeScript II 1st Strand cDNA Synthesis Kit (6210A, Takara, China). For placental tissues and PMSCs, total RNA was extracted using RNAiso Plus, and cDNA synthesis was performed via the HiScript® II Q RT SuperMix for qPCR (+gDNA wiper) (R223-01, Vazyme, China). RT-qPCR assays were carried out using ChamQ Universal SYBR QPCR Master Mix (Q711-02, Vazyme, China) (Supplementary Table S2). The RT-qPCR system and conditions are shown in Supplementary Tables S3 and S4, respectively. Data analysis was conducted using Roche software (LightCycler 480, USA), with Gapdh employed as the reference gene for data normalization. Relative gene expression levels were determined via the $2^{-\triangle\triangle Ct}$ method, and statistical analysis was performed using GraphPad Prism v.8.

Immunofluorescence staining analysis

Cells and embryos were fixed in 4% paraformaldehyde at room temperature for 20 min, followed by three 5 min washes in PBS. The samples were subsequently incubated in permeabilization solution (0.1% Triton X-100) at room temperature for 30 min, then placed in 3% BSA blocking buffer at room temperature for 1 h, followed by three 5 min washes in PBS. The samples were then incubated with primary antibodies overnight at 4°C, including anti-mouse CD105 (sc-18838; 1:100, Santa Cruz Biotechnology, USA), mouse anti-CD90 (sc-53116; 1:100, Santa Cruz Biotechnology, USA), mouse anti-CD44 (sc-7297; 1:100, Santa Cruz Biotechnology, USA), mouse anti-CD29 (sc-374429; 1:100, Santa Cruz Biotechnology, USA), rabbit anti-YAP1 (14074; 1:200, Cell Signaling Technology, USA), and mouse anti-CCND1 (sc-8396; 1:100, Santa Cruz Biotechnology, USA). The samples were then washed three times in PBS (5 min each) and incubated with secondary antibodies, including CoraLite594-conjugated goat anti-rabbit IgG (H+L) (SA00013-4; 1:1 000, Proteintech, China) or CoraLite488-conjugated goat anti-rabbit IgG (H+L) (SA00013-2; 1:1 000, Proteintech, China), at room temperature for 1 h. After removing the secondary antibodies, the samples were washed three times in PBS (5 min each). 4’,6-Diamidino-2-phenylindole (DAPI, D9542, Sigma, USA) was added for nuclear staining, with samples incubated at room temperature in the dark for 15 min, then mounted on glass slides with a fluorescence quenching reagent. After sealing, images were captured using a confocal laser scanning microscope (Nikon A1 plus, Japan). All experiments were performed under the same conditions and parameters for each group.

For immunofluorescence of tissue sections, the paraffin-embedded sections were first deparaffinized, followed by antigen retrieval in 1× citrate buffer repair solution for 20 min. The sections were immersed in a 3% H_2O_2 solution in a light-protected environment at room temperature to block endogenous peroxidase activity. The sections were then placed in a 3% BSA solution for 1 h to block nonspecific binding and incubated overnight at 4°C with primary antibodies, including rabbit anti-YAP1 (14074; 1:200, Cell Signaling Technology, USA) and mouse anti-CCND1 (sc-8396; 1:100, Santa Cruz Biotechnology, USA), followed by incubation with fluorescent-conjugated secondary antibodies at room temperature for 1 h. Finally, the nuclei were stained with DAPI.

Western blot detection

Placental tissues were homogenized with a tissue grinder and placed in protein lysis buffer (990 μL of RIPA and 10 μL of PMSF). PMSCs were similarly collected, resuspended in protein lysis buffer, and incubated on ice for 30 min. The lysates were centrifuged at 4°C and 12 000 r/min for 30 min, and the supernatant was collected as the protein sample. Nuclear and cytoplasmic proteins were extracted using NE-PER Nuclear and Cytoplasmic Extraction Reagent (78835, Thermo, USA). Protein concentrations were determined using a Pierce™ BCA Protein Assay Kit (23225, Thermo, USA). For each sample, 30 μg of protein was mixed with 5× protein loading buffer containing DTT at a 4:1 volume ratio, boiled for 10 min, and then stored at −80°C. Proteins were separated using 10% sodium dodecyl-sulfate polyacrylamide gel electrophoresis (SDS-PAGE) based on molecular weight. After electrophoresis, the proteins were transferred to polyvinylidene fluoride (PVDF) membranes, which were blocked at room temperature in 5% skim milk solution (2.5 g of skim milk powder and 50 mL of TBST) for 1 h. The membranes were then incubated overnight at 4°C with diluted primary antibodies (see Supplementary Table S5 for details). After discarding the primary antibodies, the membranes were washed four times (5 min each) with 1× TBST wash buffer on a rocking platform, then incubated with diluted secondary

antibodies, including HRP-conjugated AffiniPure goat anti-mouse IgG (H+L) (SA00001-1; 1:5 000, Proteintech, China) and HRP-conjugated AffiniPure goat anti-rabbit IgG (H+L) (SA00001-2; 1:5 000, Proteintech, China), at room temperature on a rocking platform for 1 h. After the secondary antibodies were discarded, the membranes were washed three times (10 min each) in 1× TBST wash buffer on a rocking platform. The chemiluminescent substrate was prepared by mixing luminol reagent and peroxide solution at a 1:1 ratio (32209, Thermo, USA) and applied evenly to the membrane surface. The membranes were then enclosed in self-sealing bags, ensuring the removal of any air bubbles. Exposure was performed using a chemiluminescent gel imaging system. Images were saved in the desired format, and grayscale quantification was performed using ImageJ software.

Hematoxylin and eosin (H&E) staining and immunohistochemical analysis of bovine placental tissues

Placental tissues from both CON and SCNT cattle were embedded in paraffin, cut into 5 μm-thick sections, mounted on adhesive slides, and dried at 42°C. The sections were then subjected to a series of ethanol treatments (100%, 95%, 85%, and 70%), followed by appropriate hematoxylin staining, differentiation in 1% hydrochloric acid in ethanol (concentrated hydrochloric acid and 75% ethanol), dehydration, and the addition of eosin staining solution. After subsequent treatments in 95% and 100% ethanol and incubation in xylene, the sections were sealed with neutral resin. Immunohistochemical staining involved deparaffinization and rehydration of paraffin-embedded sections, antigen retrieval, serum blocking, incubation with primary and secondary antibodies, and immunofluorescence staining of the same sections. DAB staining reagent (AR1022, Boster, China) was added to the sections, and staining time was observed under a microscope to determine the appropriate duration. Hematoxylin was used to stain the cell nuclei, followed by differentiation and bluing with differentiation solution and bluing reagent, respectively. After dehydration, the sections were sealed, and images were obtained using a microscope (Nikon ECLIPSE 80i, Japan).

Cell proliferation assay

CON and SCNT bPMSCs were seeded in 96-well plates at a density of 2×10^3/100 μL per well and cultured at 37°C with 5% CO_2 saturation for 24, 48, 72, 96, and 120 h. At different time points, 10 μL of Cell Counting Kit-8 (CCK-8) reagent (K1018, Apexbio, USA) was added to each well, followed by 2 h of incubation in the dark at 37°C with 5% CO_2. Optical density (OD) at 450 nm was subsequently measured using a microplate reader (Thermo, USA). Following the manufacturer's instructions, bPMSC proliferation was assessed using an EdU Imaging Kit (Cy3) (K1075, Apexbio, USA). EdU was added to the culture medium of both CON and SCNT bPMSCs, which were subsequently incubated overnight to label the cells. The cells were then fixed with 4% paraformaldehyde at room temperature for 15 min, followed by permeabilization with 0.5% Triton X-100 at room temperature for 20 min. The cells were subsequently incubated with 1× EdU buffer additive working solution and Click reaction solution at room temperature in the dark for 30 min. Finally, the cell nuclei were stained with DAPI, and image acquisition was performed via confocal microscopy (Nikon A1R, Japan).

Flow cytometry was used to analyze the cell cycle of the bPMSCs. Initially, cells were collected and placed in prechilled 70% ethanol for overnight fixation at 4°C. The cells were then incubated in a premade propidium iodide staining solution at 37°C for 30 min in the dark. Cell cycle analysis was carried out using a Cytoflex flow cytometer, and the percentages of cells in the G0/G1 and S phases were calculated and analyzed with FlowJo software.

Chromatin Immunoprecipitation (ChIP) and ChIP-qPCR analysis

ChIP was conducted using a Simple ChIP Plus Enzymatic Chromatin IP Kit (9005, Cell Signaling Technology, USA), following the manufacturer's instructions. In brief, cells were exposed to 1% formaldehyde at room temperature for 10 min to cross-link chromatin, with the reaction stopped by the addition of glycine. After the samples were collected and chromatin was enzymatically fragmented using the provided mixed buffer. Agarose gel electrophoresis verified that the chromatin fragments fell within the 150–900 bp range. Fragmented chromatin was subsequently subjected to ChIP using a YAP1 antibody (14074, Cell Signaling Technology, USA, 14074, 10 μg/tube) and IgG (included in the kit, 2 μg/tube). Precipitated DNA samples were quantified using quantitative real-time PCR (qPCR), with results expressed as a percentage of input DNA.

Luciferase assay

Using the 2 000 bp upstream region of the CCND1 gene as the promoter sequence from NCBI, YAP1 binding sites on the CCND1 promoter were predicted using the JASPAR database (http://jaspar.binf.ku.dk/cgi-bin/jaspar_db.pl) and corresponding binding primers were designed accordingly (Supplementary Table S6). A recombinant plasmid containing the CCND1 luciferase reporter gene was subsequently constructed using the psiCHECK-2 vector. The CCND1 promoter region (upstream 2 000 bp) was divided into three segments based on predicted binding sites: (-579-1), (-1458-579), and (-2000-1458). Recombinant plasmids psiCHECK-2-pCCND1, psiCHECK-2-(pCCND1-579-1), psiCHECK-2-(pCCND1-1458-579), and psiCHECK-2-(pCCND1-2000-1458) were then generated. Luciferase reporter gene activity was then measured using the Dual-Luciferase Reporter Assay System and a luminometer (Thermo, USA), following the manufacturer's instructions.

Coimmunoprecipitation detection

The bPMSCs were prepared by adding prechilled IP lysis/wash buffer, followed by incubation on ice for 5 min. Cells were then collected, sonicated, and centrifuged at 4°C and 13 000 ×*g* for 10 min. The resulting supernatant was used to determine protein concentration. Immunoprecipitation was conducted using a Pierce Co-Immunoprecipitation (Co-IP) Kit (26149, Thermo, USA) according to the manufacturer's instructions. Antibodies were incubated with the resin and covalently crosslinked. The antibody-conjugated resin was then incubated with 200 μL of bPMSC protein lysate at 4°C overnight. After washing, the antibody-bound protein complexes were eluted, and protein blot analysis was performed as described previously.

Quantification and statistical analysis

All values are expressed as means ± standard error of the mean (SEM). GraphPad Prism v.8 was used to analyze the significance of differences, with one-way analysis of variance

(ANOVA) used for multiple group comparisons and Student's *t*-test used for two-group comparisons. *P*-values less than 0.05 were considered statistically significant (*: $P<0.05$; **: $P<0.01$; ***: $P<0.001$, or as indicated in the figure legends). All experiments were repeated three times for both technical and biological replicates.

RESULTS

Abnormal placental tissue and placental RNA-seq analysis in SCNT cattle

Comparative analysis of cloned and CON cattle during gestation and the perinatal period revealed that cloned cattle experienced prolonged gestation periods, increased abdominal circumferences during the perinatal period, and significantly higher birth weights of SCNT calves (Supplementary Figure S1A–F). Postpartum assessment of placental cotyledons demonstrated a significant reduction in cotyledon number in SCNT cattle ($P<0.05$), accompanied by a marked increase in cotyledon length and width ($P<0.001$) (Figure 1A–D; Supplementary Figure S1C). Histological examination indicated substantial changes, including a significant increase in binucleate trophoblast giant cells within SCNT placental tissue, disordered arrangement of uterine epithelial cells (UE), and a significant increase in interstitial villi within the chorionic membrane (Figure 1E, F; Supplementary Figure S1G). To investigate the underlying molecular mechanisms contributing to placental enlargement in SCNT cattle, RNA-seq was performed on SCNT placental tissue, identifying many DEGs. These DEGs were primarily involved in biological functions such as cell morphogenesis, cell motility, cell migration, cell localization, cellular stress response, cell cycle, and cytoskeletal organization (Supplementary Figure S1H, I). These genes were also significantly enriched in the PI3K-AKT and Hippo pathways (Figure 1G), suggesting a potential link between placental overgrowth in cloned cattle and dysregulated gene expression within these pathways. Focusing on genes with co-regulatory roles in both the PI3K-AKT and Hippo pathways, further analysis identified three genes with significant differential expression, including cyclin D1 (*Ccnd1*), protein phosphatase 2 regulatory subunit B (*Ppp2r2b*), and fibroblast growth factor 1 (*Fgf1*), with *Ccnd1* exhibiting the most pronounced expression change (Figure 1H–J; Supplementary Figure S1J, K).

Colocalized expression regulation analysis of *Yap1* and *CCND1* in SCNT and CON cattle placental tissues

To explore the regulatory mechanisms behind placental enlargement in SCNT cattle, bPMSCs were isolated from both SCNT and CON cattle for experimental analysis. The isolated bPMSCs exhibited a spindle-like elongated morphology and a whirlpool-like growth pattern (Supplementary Figure S2A). Surface marker profiling confirmed these cells were positive for CD29, CD44, CD90, and CD105 but negative for the hematopoietic stem cell marker CD34 (Supplementary Figure S2B). Furthermore, these bPMSCs successfully differentiated into osteogenic and adipogenic lineages *in vitro* (Supplementary Figure S2C, D), validating their suitability for further experimental research.

Given the significant enrichment of the Hippo and PI3K-AKT signaling pathways observed in the RNA-seq data from SCNT placental tissues, further research was conducted on two key regulatory factors within these pathways, *Yap1* and *Ccnd1*. The Hippo pathway is known to influence organ size and volume, while CCND1 plays a critical role in cell cycle regulation (Cheraghi et al., 2015; Heallen et al., 2011). Immunofluorescence analysis demonstrated colocalization of Yap1 and CCND1 in SCNT and CON placental tissues (Figure 2A), bPMSCs (Figure 2C), and preimplantation blastocysts (Figure 2E), with higher immunofluorescence intensities for YAP1 and CCND1 in the SCNT groups (Figure 2B, D, F). Immunohistochemical analyses further corroborated these findings, showing significantly elevated YAP1 and CCND1 protein levels in SCNT placental tissues compared to the CON group (Supplementary Figure S3A, B). RT-qPCR analysis confirmed that *Yap1* and *Ccnd1* expression levels in SCNT placental tissues, bPMSCs, and preimplantation blastocysts were significantly higher than in the CON group (Supplementary Figure S3C–E). Additionally, stage-specific Immunofluorescence of YAP1 during preimplantation embryo development revealed prominent nuclear expression. Specifically, YAP1 expression was significantly elevated at the 8-cell stage compared to the CON group and further increased at the 16-cell and blastocyst stages (Supplementary Figure S3F, G). These results demonstrate that YAP1 and CCND1 are expressed at higher levels in the placental tissues, bPMSCs, and preimplantation embryos of the SCNT group compared to the CON group, with these expression differences emerging in the early developmental stages of the cloned embryos.

Elevated YAP1 and CCND1 expression in SCNT bPMSCs and cell proliferation and cell cycle regulation

The above findings demonstrated that YAP1 and CCND1 exhibit colocalized expression patterns in tissues, bPMSCs, and embryos. Given that YAP1 regulates cell proliferation and cell cycle progression, impacting organ size (Heallen et al., 2011), we further investigated whether YAP1 regulates CCND1 and subsequently affects cell proliferation in SCNT-derived bPMSCs, potentially contributing to abnormal placental development in cloned cattle.

Fluorescence EdU analysis revealed a significantly higher proportion of newly synthesized DNA in SCNT bPMSCs compared to CON bPMSCs ($P<0.01$), indicating a markedly enhanced proliferative capacity in the SCNT group (Figure 3A, B). Cell cycle analysis showed a significant reduction in the proportion of SCNT bPMSCs in the G0/G1 phase and a corresponding increase in the S-phase population relative to CON bPMSCs (Figure 3C; Supplementary Figure S4A). To further assess proliferation dynamics, CCK-8 assays were conducted at 0, 24, 48, 72, 96, and 120 h. At 24 h, no significant difference was observed between SCNT and CON bPMSCs ($P>0.05$); however, SCNT bPMSCs displayed significantly enhanced proliferation at 48–72 h ($P<0.05$) and at 96–120 h ($P<0.01$) (Figure 3D). Collectively, these findings suggest that SCNT bPMSCs exhibit accelerated cell division and proliferative capacity.

Previous research has shown that the YAP1 protein, when dephosphorylated, is translocated into the nucleus, where it activates the transcription of downstream target genes, driving cell growth, proliferation, differentiation, and migration (Mizuno et al., 2012). To investigate YAP1 signaling in SCNT and CON bPMSCs and placental tissues, we analyzed the distribution and phosphorylation status of YAP1 in both the cytoplasm and nucleus. Western blot analysis revealed a significant increase

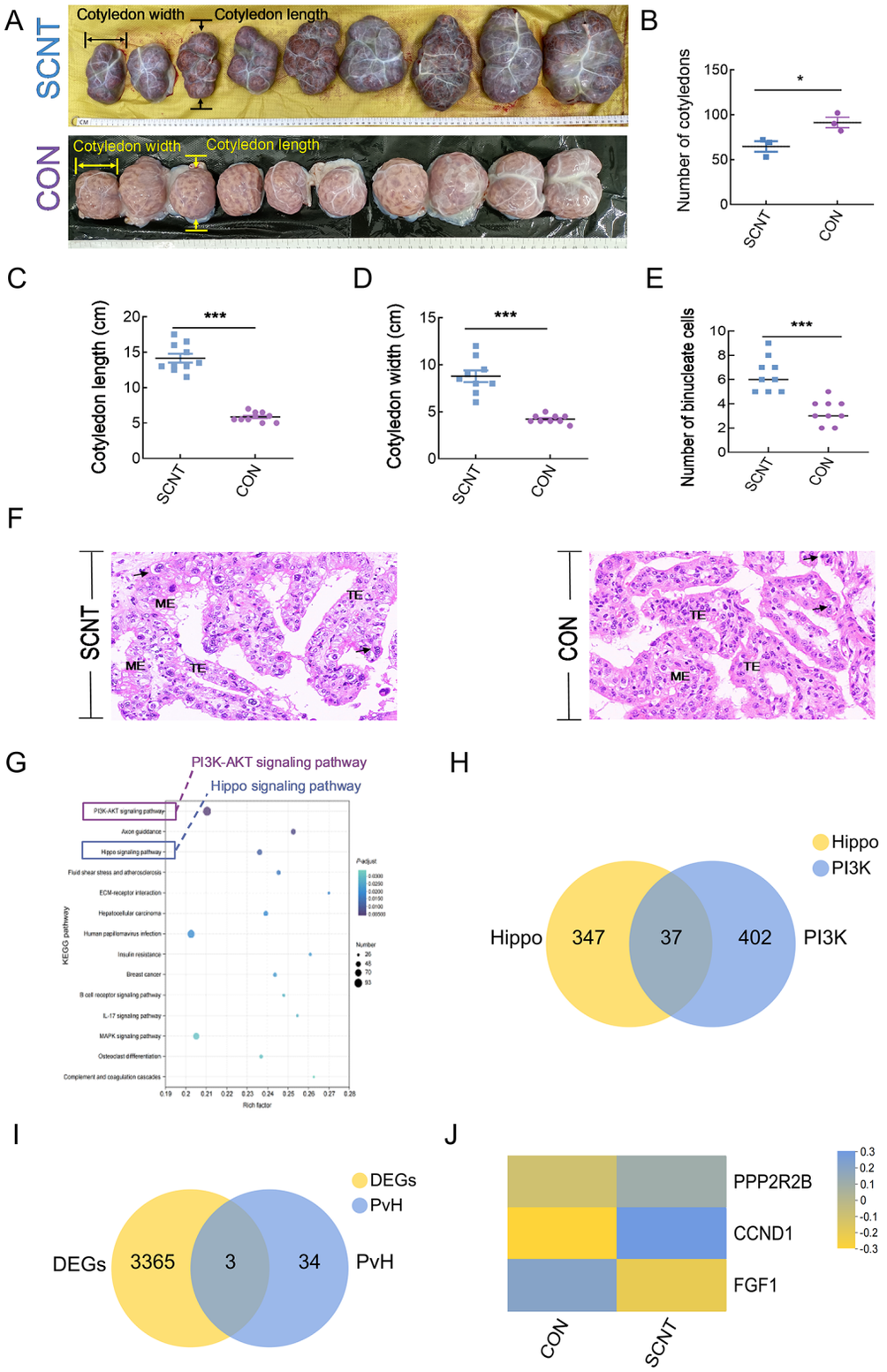

Figure 1 Morphological analysis of placental tissues and RNA-seq transcriptome of cloned and control (CON) cattle

A: Morphological size and distribution of placental cotyledons in SCNT and CON groups. B: Statistical analysis of number of placental cotyledons in SCNT and CON groups. C: Comparison of cotyledon length between SCNT and CON groups. D: Comparison of cotyledon width between SCNT and CON groups. E: Statistical analysis of number of binucleated cells in SCNT and CON bovine placentas. F: Histological staining of chorionic membrane structure in SCNT and CON bovine placentas (H&E staining, TE, trophoblast epithelium; ME, mesenchyme; arrows, binucleate giant cells); Scale bars: 100 μm. G: KEGG enrichment analysis of DEGs in placental tissues of SCNT and CON groups. H: Significant DEGs involved in PI3K-AKT and Hippo signaling pathways in placental tissues of SCNT and CON groups. I: Selection of significant DEGs commonly regulated in PI3K-AKT and Hippo signaling pathways in placental tissues of SCNT and CON groups. J: Cluster analysis of *CCND1*, *PPP2R2B*, and *FGF1* genes in placental tissues of SCNT and CON groups. Graphs show mean±SEM, data are representative of three independent experiments. “PvH” refers to DEGs within PI3K-Akt and Hippo signaling pathways. *: P<0.05; **: P<0.01; ***: P<0.001; ns: Not significant.

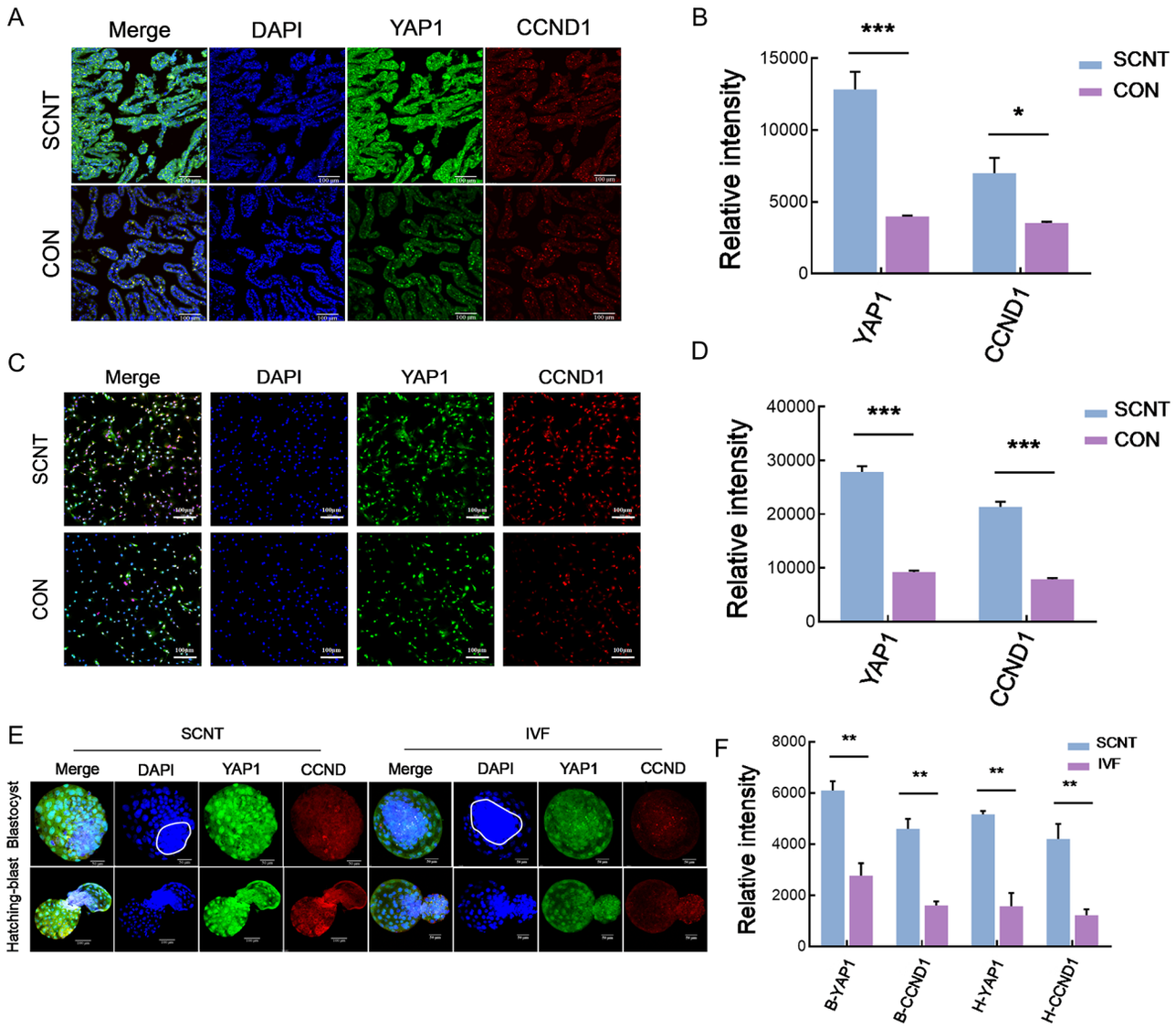

Figure 2 Detection of YAP1 and CCND1 expression levels in placental tissues, bPMSCs, and blastocyst-stage embryos of SCNT and IVF groups

A: Immunofluorescence (IF) detection of YAP1 and CCND1 protein expression in SCNT and CON placental tissues; Scale bars: 100 μm. B: IF relative intensity analysis of YAP1 and CCND1 in SCNT and CON placental tissues. C: IF detection of YAP1 and CCND1 expression in bPMSCs of SCNT and CON groups; Scale bars: 200 μm. D: IF relative intensity analysis of YAP1 and CCND1 in bPMSCs of SCNT and CON groups. E: IF detection of YAP1 and CCND1 expression in SCNT and IVF blastocysts; inner cell mass (ICM) region of blastocysts is marked with a white circle. Scale bars: 50 μm. F: IF relative intensity analysis of YAP1 and CCND1 in SCNT and IVF blastocysts. Graphs show mean±SEM, data are representative of three independent experiments. *: P<0.05; **: P<0.01; ***: P<0.001.

in YAP1 and CCND1 protein expression in SCNT bPMSCs (P<0.001). Nuclear YAP1 (Nuc-YAP1) and cytoplasmic YAP1 (Cyto-YAP1) levels in SCNT bPMSCs were significantly higher than those in the CON group (P<0.05), while phosphorylated YAP1 at serine 127 (P-YAP1-S127) and serine 397 (P-YAP1-S397) was significantly lower (Figure 3E, F). These findings were validated in placental tissue, which showed consistent expression trends at the cellular level (Supplementary Figure S4B, C). These results indicate that YAP1 levels are significantly higher in SCNT bPMSCs than in CON bPMSCs, with reduced phosphorylation, suggesting increased nuclear localization and functional activity of YAP1. The expression of CCND1 in SCNT bPMSCs showed a similar trend to that of YAP1, further suggesting a positive regulatory relationship between YAP1 and CCND1 in these cells.

To further explore the mechanisms driving cell proliferation, we examined cyclin-dependent kinases (CDKs), cell cycle inhibitory genes, and proliferation markers known to influence this process. CCND1, as a regulatory subunit, forms complexes with CDK4 or CDK6 (Aggarwal et al., 2010). These cyclin-dependent kinases are indispensable for G1 to S phase transition. CCND1 is also recognized as an oncogene, and its overexpression can lead to uncontrolled cell proliferation and malignancy (Wang et al., 2006; Zhong et al., 2010). Here, RT-qPCR and western blot analyses confirmed significant up-regulation of cell proliferation-related proteins, including CDK4, CDK6, proliferating cell nuclear antigen (PCNA), MYC proto-oncogene, Bhlh transcription factor (C-MYC), and Ki-67 (Ki67) in the SCNT group. Conversely, the expression of cyclin-inhibiting genes, such as cyclin-dependent kinase inhibitor 2A (CDKN2A), CDKN2B, and CDKN2C, was significantly down-regulated in the SCNT group (Figure 3G–I).

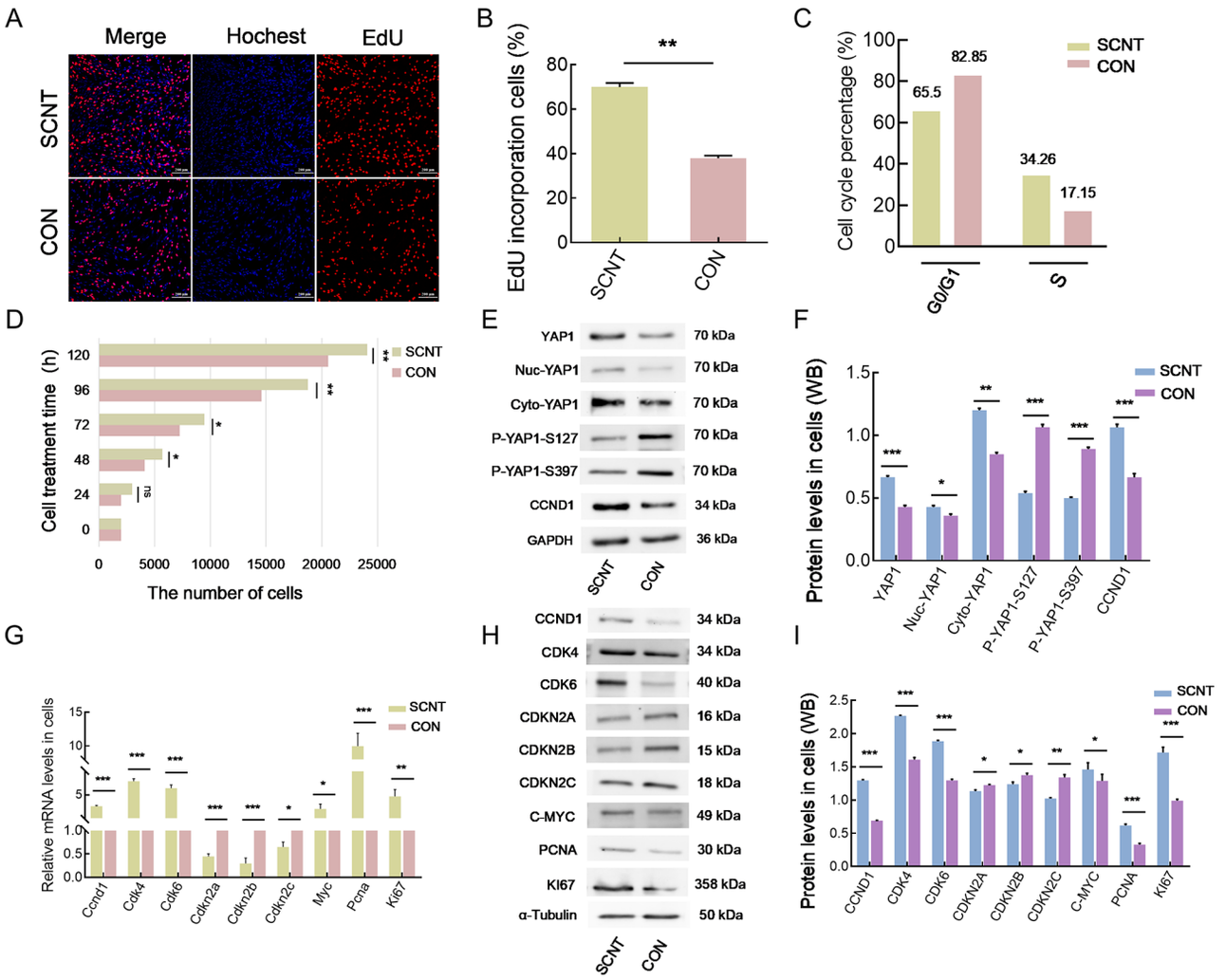

Figure 3 Proliferation analysis of bPMSCs and expression analysis of cell cycle-related genes in SCNT and CON groups

A: EdU proliferation assay of SCNT and CON bPMSCs. Scale bars: 200 μm. B: Statistical analysis of EdU proliferation data in SCNT and CON bPMSCs. C: Cell cycle distribution analysis of SCNT and CON bPMSCs. D: Proliferation assay of SCNT and CON bPMSCs at 0, 24, 48, 72, 96, and 120 h by CCK-8 assay, respectively. E: Western blot analysis of CCND1, YAP1, and phosphorylated YAP1 protein levels in SCNT and CON bPMSCs, respectively. F: Grayscale analysis of CCND1, YAP1, and phosphorylated YAP1 proteins in SCNT and CON bPMSCs. G: RT-qPCR analysis of mRNA expression levels of cell cycle-related genes (*Ccnd1*, *Cdk4*, *Cdk6*, *Cdkn2a*, *Cdkn2b*, *Cdkn2c*, *Myc*, *Pcna*, and *Ki67*) in SCNT and CON bPMSCs. H: Western blot analysis of protein expression levels of cell cycle-related proteins (CCND1, CDK4, CDK6, CDKN2A, CDKN2B, CDKN2C, MYC, PCNA, and KI67) in SCNT and CON bPMSCs. I: Grayscale analysis of cell cycle-related proteins in SCNT and CON bPMSCs. Graphs show mean±SEM, data are representative of three independent experiments. *: $P<0.05$; **: $P<0.01$; ***: $P<0.001$; ns: Not significant.

In summary, SCNT bPMSCs presented enhanced DNA synthesis, accelerated cell cycle progression, and increased expression of CCND1-associated cyclin-dependent kinases and proliferation-related genes compared to CON bPMSCs.

Regulation of YAP1 gene expression affects bPMSC proliferation

In light of the colocalization relationship between CCND1 and YAP1, we further investigated whether YAP1 regulates the proliferation of bPMSCs in cloned cattle and its potential interaction with CCND1. Overexpression and knockdown vectors for YAP1 were first constructed and transfected into SCNT and CON bPMSCs, establishing YAP1-overexpressing ($CON^{OE\text{-}YAP1}$) and YAP1-knockdown ($CON^{sh\text{-}YAP1}$, $SCNT^{sh\text{-}YAP1}$) bPMSCs for subsequent validation studies (Supplementary Figure S5A, B). Western blot and qPCR analyses confirmed successful YAP1 transfection in bPMSCs, showing a significant increase in YAP1 mRNA and protein expression levels in both the nucleus and cytoplasm of $CON^{OE\text{-}YAP1}$ cells (Supplementary Figure S5C–F). Furthermore, four YAP1-targeted shRNAs were designed, and the lentiviral-mediated plasmid pLKO.1-copGFP-shYAP1 was transfected into SCNT/CON bPMSCs. Of these, shYAP1-4 exhibited the highest efficiency in inhibiting YAP1 mRNA and protein expression, allowing the selection of stably transfected $SCNT^{sh\text{-}YAP1}$ and $CON^{sh\text{-}YAP1}$ cell lines via puromycin treatment. Additionally, the application of the YAP1 inhibitor verteporfin in SCNT bPMSCs restored YAP1 expression to levels comparable to those in the CON group (Supplementary Figure S5C–E).

The proliferation capacities of $SCNT^{sh\text{-}YAP1}$, $SCNT^{Verteporfin}$, $CON^{OE\text{-}YAP1}$, $CON^{sh\text{-}YAP1}$, and $CON^{Verteporfin}$ bPMSCs were assessed and compared to CON and SCNT bPMSCs. Results indicated that the proportion of newly synthesized DNA to total DNA in $CON^{OE\text{-}YAP1}$ bPMSCs was significantly higher than that in CON bPMSCs and similar to the level observed in SCNT bPMSCs. In contrast, the proportion of newly synthesized

DNA to total DNA in $CON^{sh\text{-}YAP1}$ and $CON^{Verteporfin}$ bPMSCs was significantly lower than in CON bPMSCs. Additionally, the proportion of newly synthesized DNA to total DNA in $SCNT^{sh\text{-}YAP1}$ and $SCNT^{Verteporfin}$ bPMSCs was significantly lower than that in SCNT bPMSCs and similar to the levels observed in CON bPMSCs (Figure 4A, B). Further proliferation assays over 24, 48, 72, 96, and 120 h revealed that the $CON^{OE\text{-}YAP1}$ bPMSCs displayed a significantly enhanced proliferative capacity compared to CON bPMSCs, similar to that of SCNT bPMSCs. Conversely, both $CON^{sh\text{-}YAP1}$ and $CON^{Verteporfin}$ bPMSCs demonstrated significantly lower proliferative capacity than that of CON (Figure 4C). Additionally, the proliferative capacity of $SCNT^{sh\text{-}YAP1}$ and $SCNT^{Verteporfin}$ bPMSCs was significantly lower than that of SCNT bPMSCs and similar to that of CON bPMSCs (Figure 4C). RT-qPCR analysis of cell cycle and cell proliferation-related gene expression in $CON^{OE\text{-}YAP1}$ bPMSCs revealed up-regulation of *Ccnd1*, *Cdk4*, *Cdk6*, *Myc*, *Pcna*, and *Ki67* to levels comparable to those in SCNT bPMSCs. Simultaneously, the expression levels of *Cdkn2a*, *Cdkn2b*, and *Cdkn2c* were reduced (Supplementary Figure S5G).

Cell cycle analysis revealed that the proportion of $CON^{OE\text{-}YAP1}$ bPMSCs in the G0/G1 phase was significantly lower than that of CON bPMSCs, while the proportion of cells in the S phase was significantly higher, similar to the distribution observed in SCNT bPMSCs. Conversely, the proportion of cells in the G0/G1 phase in $CON^{sh\text{-}YAP1}$ and $CON^{Verteporfin}$ bPMSCs was significantly higher than that in CON bPMSCs, while the proportion of cells in the S phase was significantly lower. In $SCNT^{sh\text{-}YAP1}$ and $SCNT^{Verteporfin}$ bPMSCs, the proportion of cells in the G0/G1 phase was significantly higher than that in SCNT bPMSCs, while the proportion of cells in the S phase was significantly lower, similar to the distribution observed in CON bPMSCs (Figure 4D; Supplementary Figure S6).

YAP1-mediated regulation of CCND1 expression in bPMSCs

Considering the proliferative effect of YAP1 overexpression and the inhibitory effect of YAP1 knockdown on bPMSCs, we conducted RT-qPCR and western blot analyses to further confirm the impact of YAP1 expression changes on CCND1 expression. In CON, $CON^{OE\text{-}YAP1}$, $CON^{sh\text{-}YAP1}$, and $CON^{Verteporfin}$ bPMSCs, YAP1 and CCND1 mRNA and protein expression levels followed a similar expression pattern (Figure 5A–C). However, YAP1 knockdown in SCNT bPMSCs led to a significant down-regulation in CCND1 expression, similar to the levels observed in CON bPMSCs (Figure 5D–F). These findings indicate that YAP1 positively regulates CCND1 expression in bPMSCs.

To further validate the specific regulatory relationship between YAP1 and CCND1, Co-IP, luciferase, and ChIP-qPCR assays were conducted. The Co-IP results demonstrated co-expression of YAP1 and CCND1 protein in bPMSCs (Input). In control assays using IgG, neither YAP1 nor CCND1 was precipitated, indicating that these proteins did not bind to IgG. However, immunoprecipitation targeting the YAP1 protein successfully precipitated CCND1 (Figure 5G), and vice versa (Figure 5H), indicating a direct interaction between YAP1 and CCND1 proteins.

The impact of *Yap1* on *Ccnd1* promoter activity was assessed using a dual-luciferase reporter system, with the *Ccnd1* promoter inserted into the psiCHECK-2 vector. SCNT bPMSCs with elevated *Yap1* expression exhibited significantly increased activity of the psiCHECK-2-pCCND1 and psiCHECK-2-(pCCND1-1458-579) promoters, with the psiCHECK-2-(pCCND1-579-1) promoter showing a marked increase. However, no significant activity change was observed with the psiCHECK-2-(pCCND1-2000-1458) promoter. In SCNT bPMSCs, *Ccnd1* promoter activity was significantly increased, indicating that YAP1 has a promoting effect on the *Ccnd1* promoter (Figure 5I). These findings suggest that YAP1 promotes *Ccnd1* expression by binding to the proximal promoter (pCCND1-579-1). ChIP-qPCR analysis confirmed increased YAP1 binding to the *Ccnd1* promoter in SCNT bPMSCs with elevated YAP1 expression (Figure 5J). These results indicate that YAP1 up-regulates *Ccnd1* expression by binding directly to its proximal promoter.

YAP1 promotes G0/G1-S transition in bPMSCs via the CCND1-CDK6 pathway

To further investigate the mechanism by which YAP1 promotes SCNT bPMSC proliferation through CCND1 up-regulation, we exposed SCNT bPMSCs to the CDK4/CDK6 inhibitor BSJ-03-204 (inhibitory concentrations of 26.9 nmol/L for CDK4/CCND1 and 10.4 nmol/L for CDK6/CCND1) and assessed their cell proliferative capacity. Western blot and RT-qPCR analyses demonstrated that YAP1 overexpression in the CON group led to increased CDK4 and CDK6 expression (Figure 6A–C). Furthermore, inhibition of CDK6 (SCNT-CDK6) significantly reduced the proportion of S-phase cells among SCNT bPMSCs, resulting in proliferation levels similar to those observed in CON bPMSCs. Inhibition of CDK4 (SCNT-CDK4) also reduced the proportion of S-phase cells, although the effect was less pronounced than that of CDK6 (Figure 6D–F). These findings indicate that YAP1 drives the G0/G1-S phase transition in SCNT bPMSCs predominantly via the CCND1-CDK6 pathway.

DISCUSSION

SCNT has emerged as a valuable and promising tool with significant implications for agricultural and medical applications. Advances in SCNT and related biotechnology have played a critical role in germplasm conservation, maintaining genetic diversity and enhancing adaptability in agricultural species. Despite the potential benefits offered by assisted reproductive technologies in cattle, pregnancies derived from cloning technologies present numerous challenges, including abnormal placental phenotypes and health issues in newborns and surrogate mothers. Furthermore, the reproductive efficiency of SCNT remains suboptimal, with success rates consistently below 5%, compounded by low pregnancy rates, high incidences of pregnancy loss, and a multitude of fetal and placental abnormalities (Arnold et al., 2008; Matoba & Zhang, 2018; Yang et al., 2007). In SCNT mouse models, placental tissues exhibit pronounced trophoblast layer expansion, accompanied by destruction of the labyrinth layer, trophoblast cell hypertrophy, and abnormal increase in glycogen cell number, ultimately resulting in the abnormal proliferation of placental tissue (Wakisaka-Saito et al., 2006; Whitworth & Prather, 2010). Similarly, morphological analyses of SCNT-derived pig placentas have highlighted severe abnormalities, including reduced columnar epithelial cells, decreased placental villi density, underdeveloped nutritive layer cells, impaired vascularization, and reduced placental weight (Chae et al.,

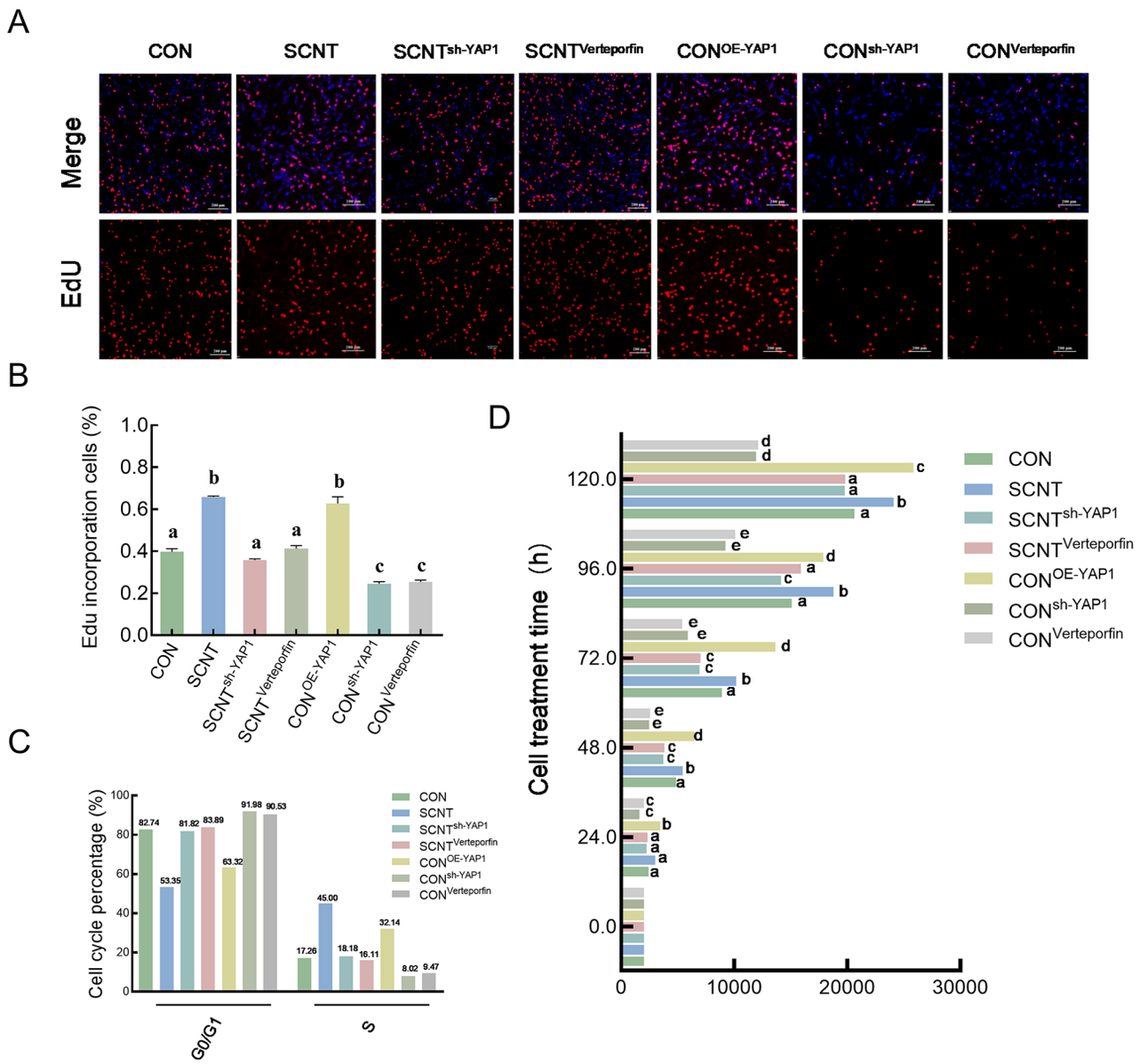

Figure 4 YAP1 promotes bPMSC proliferation

A: Proliferative capacity assay of different YAP1 overexpression and YAP1 gene knockout bPMSC groups by EdU. Scale bars: 200 μm. B: Statistical analysis of proliferation detected by EdU assay in bPMSCs with YAP1 overexpression and YAP1 gene knockout. C: Proliferation assay of different YAP1 overexpression and YAP1 gene knockout bPMSC groups by CCK-8 method at 0, 24, 48, 72, 96, and 120 h, respectively. D: Statistical analysis of cell cycle distribution in different YAP1 overexpression and YAP1 gene knockout bPMSCs groups. sh-YAP1 and verteporfin represent down-regulation of YAP1 expression, while OE-YAP1 represents overexpression of YAP1.Graphs show mean±SEM, data are representative of three independent experiments. Same letters indicate no significant differences (P>0.05), and different letters indicate significant differences (P<0.05).

2006; Lee et al., 2007; Park et al., 2009). In SCNT-derived cattle, placental abnormalities are also present and widespread. Notably, over 50% of pregnancies result in miscarriage during the first trimester (Hill et al., 2000). Furthermore, early-stage pregnancies frequently exhibit reduced placental cotyledons, increased placental dysplasia, and reduced vascularization (Hill, 2014). Between days 30 and 90 of gestation, SCNT-derived bovine placentas often show abnormal villous epithelium development, allantoic dysplasia, and vascular defects, leading to a decrease in cotyledon number (Biase et al., 2016; Chavatte-Palmer et al., 2006). Between days 100 and 150, cotyledon count in cloned bovine placentas decreases further, while uterine caruncle weight increases significantly (Chavatte-Palmer et al., 2006). In addition, crypt expansion on the caruncle surface aggregates individual villi into composite structures, further exacerbating placental abnormalities (Miglino et al., 2007).

In this study, SCNT cattle exhibited significantly prolonged gestation periods and markedly increased abdominal circumference during the perinatal period. Birth weights of SCNT calves were significantly higher than those in the CON group. Additionally, morphological analysis of SCNT placentas revealed a substantial reduction in the number of cotyledons (>2 cm), accompanied by a significant increase in cotyledon length and width. Histological assessment of placental tissue identified several abnormalities, including a significant increase in binucleate giant cells, disordered arrangement of cuboidal uterine epithelial cells, and a pronounced increase in

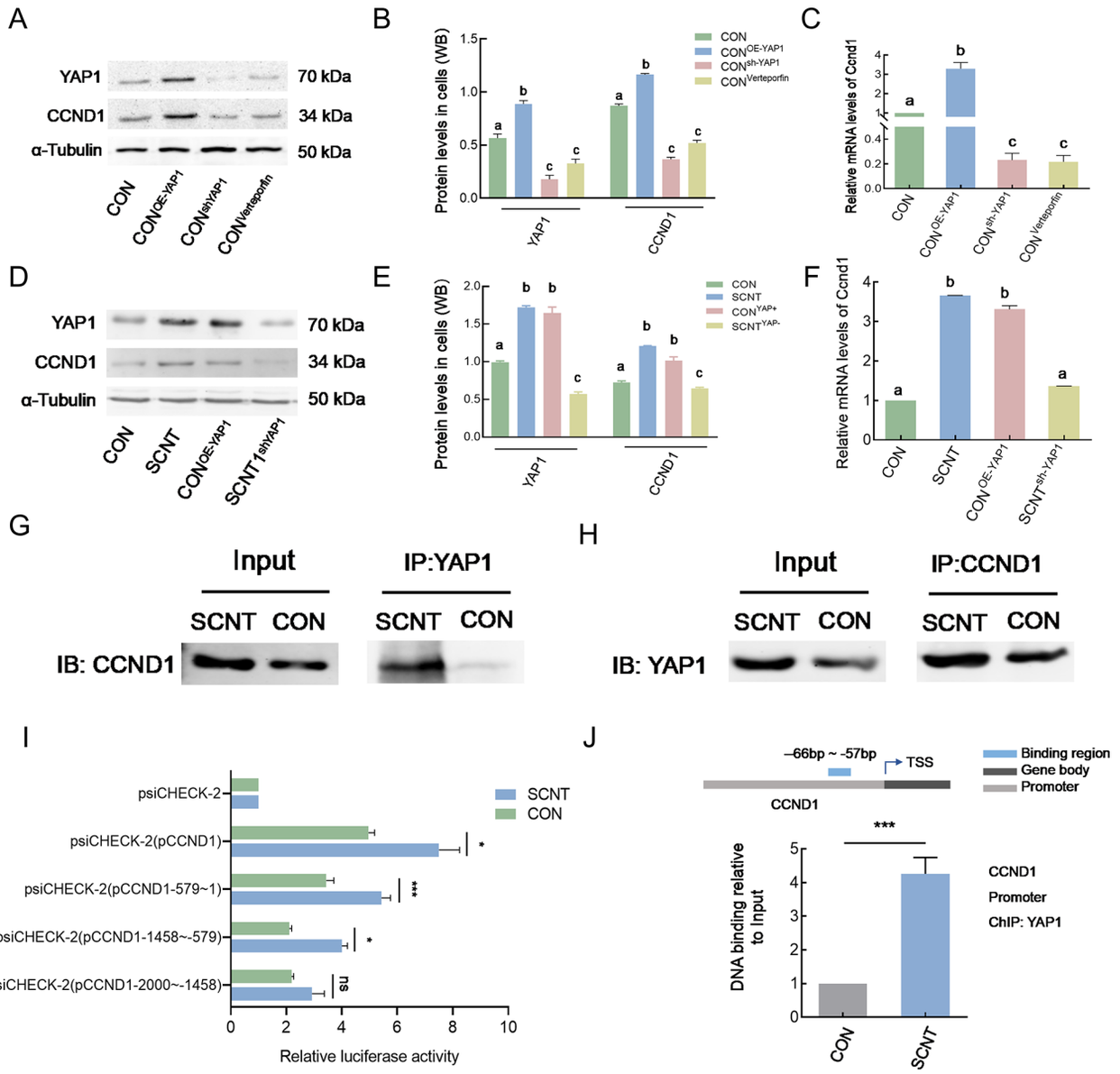

Figure 5 Regulatory role of YAP1 and CCND1 in bPMSCs

A: Western blot analysis of CCND1 protein expression in CON bPMSCs with YAP1 gene overexpression or knockout. B: Quantitative analysis of CCND1 protein expression in CON bPMSCs using densitometry (gray intensity analysis). C: RT-qPCR detection of *CCND1* mRNA expression in CON bPMSCs with *YAP1* gene overexpression or knockout. D: Western blot analysis of CCND1 protein expression in bPMSCs with YAP1 gene overexpression or knockout. E: Quantitative analysis of CCND1 protein expression in bPMSCs by densitometry. F: qPCR detection of *CCND1* mRNA expression in bPMSCs with YAP1 gene overexpression or knockout. G: Immunoprecipitation of YAP1 protein in bPMSCs. H: Immunoprecipitation of CCND1 protein in bPMSCs. I: Dual-luciferase reporter assay to validate promoting effects of YAP1 on CCND1 promoter activity. J: Chromatin immunoprecipitation (ChIP) verification of YAP1 binding to CCND1 promoter. sh-YAP1 and verteporfin represent down-regulation of YAP1 expression, while OE-YAP1 represents overexpression of YAP1. Graphs show mean±SEM, data are representative of three independent experiments. Different significance levels are indicated by asterisks (*: P<0.05; **: P<0.01; ***: P<0.001; ns: Not significant).

cotyledon interstitial villi. Cattle and other ruminants possess cotyledonary placentas, wherein placental functionality depends on the proper formation and arrangement of cotyledons and uterine caruncles. During SCNT pregnancies, the number of placental cotyledons is significantly reduced, alongside a noticeable enlargement of uterine caruncles (Fletcher et al., 2007; Young et al., 1998). This reduction in placental cotyledons, coupled with caruncular hypertrophy, likely reflects compromised placental function, which may contribute to developmental abnormalities in cloned fetuses (Fletcher et al., 2007; Young et al., 1998). The increase in binucleate giant cells in SCNT placentas likely results from an increase in the number of trophoblast cells from the fetal-nourishing outer layer and maternal uterine epithelial cells, leading to placental enlargement, thickening, and a characteristic fist-like morphology (Lee et al., 2004; Ravelich et al., 2006). The disordered arrangement of uterine epithelial cells in SCNT-derived cattle may disrupt metabolic processes, impairing placental function (Constant et al., 2006; Pool et al., 2019). Mesenchymal tissue, a key regulator of organ-specific morphogenesis, exhibits marked alterations in SCNT cattle (Constant et al., 2006; Pool et al., 2019). Specifically, the significant increase in chorionic interstitial villi suggests potential stromal regulatory mechanisms contributing to

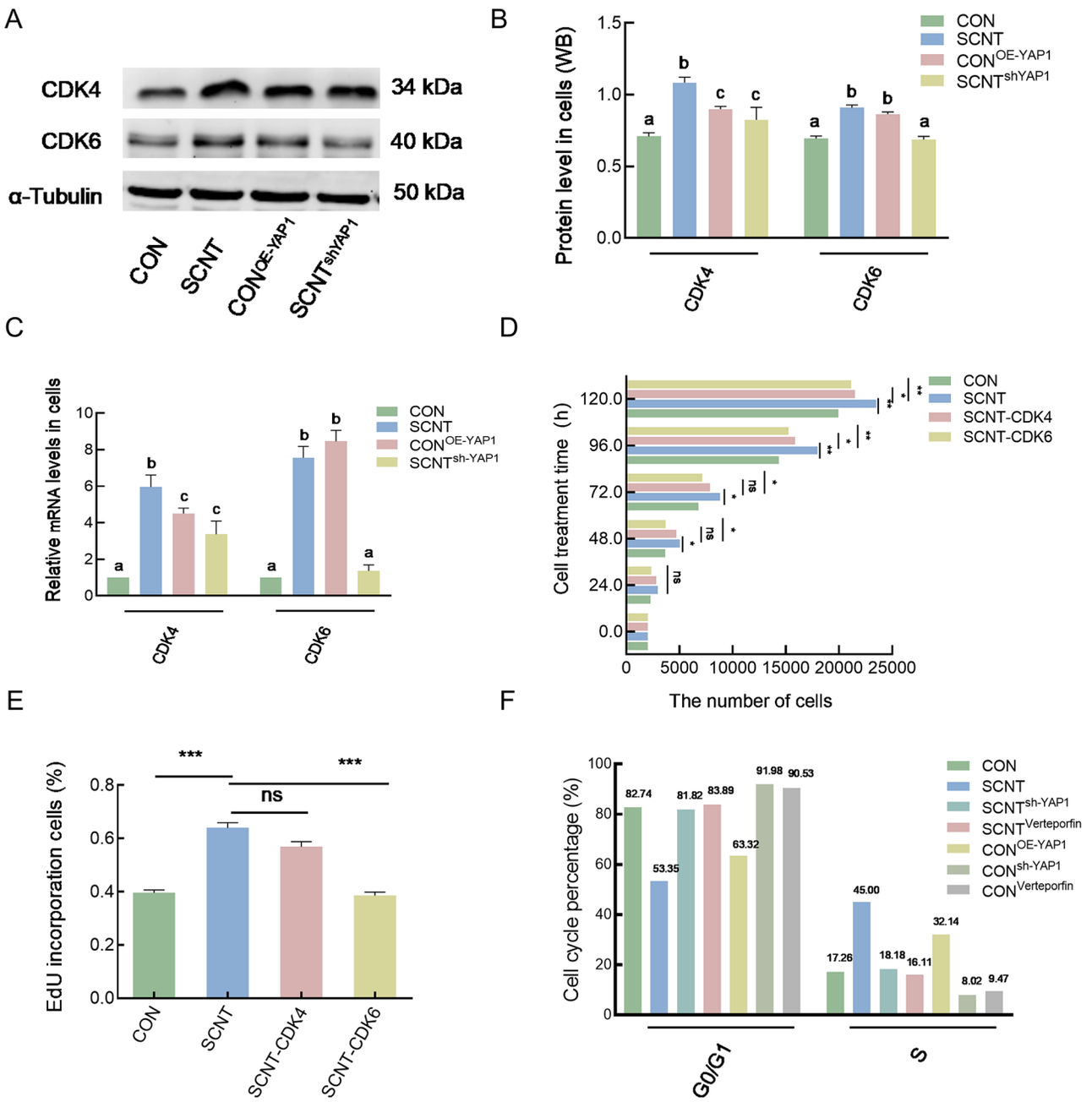

Figure 6 YAP1 promoted G0/G1-S transition of bPMSCs through CCND1-CDK6 pathway

A: Western blot analysis of CDK4 and CDK6 protein expression in bPMSCs with YAP1 gene overexpression or knockout. B: Quantitative analysis of CDK4 and CDK6 protein expression in bPMSCs by densitometry. C: RT-qPCR detection of *CDK4* and *CDK6* mRNA expression in bPMSCs with YAP1 gene overexpression or knockout. D: Proliferation assessment of bPMSCs treated with BSJ-03-204 (CDK4 26.9 nmol/L, CDK6 10.4 nmol/L) at 0, 24, 48, 72, 96, and 120 h by CCK-8 method. E: EdU proliferation assay of bPMSCs. F: Cell cycle analysis of bPMSCs. sh-YAP1 represents down-regulation of YAP1 expression, while OE-YAP1 represents overexpression of YAP1. Graphs show mean±SEM, data are representative of three independent experiments. Significance levels are indicated by asterisks (*: P<0.05; **: P<0.01; ***: P<0.001; ns: Not significant). Different letters denote significant differences (P<0.05) between groups.

placental hypertrophy (Constant et al., 2006; Pool et al., 2019). Placental overgrowth may precede and potentially drive fetal overgrowth, suggesting that fetal overgrowth may arise as a consequence rather than a cause of placental hypertrophy. Overall, these findings indicate that SCNT placental tissues in cattle exhibit pronounced abnormalities characteristic of large offspring syndrome and large placental syndrome. These abnormalities are closely associated with disrupted placental structure and function, potentially driven by metabolic dysregulation and aberrant cell signaling.

Previous studies have identified multiple factors contributing to placental hypertrophy in SCNT animals, including abnormal imprinting gene expression, dysregulated hormone secretion, epigenetic modifications, RNA dysregulation, and abnormal signal regulation. Abnormal gene expression during placental development has been highlighted as a major driver of pathological changes in cloned placentas (Inoue et al., 2002; Rivera, 2021). Everts et al. (2008) reported that DEGs in the developing placenta of SCNT bovines are enriched in cell cycle regulation and apoptosis. Similarly, Salilew-Wondim

et al. (2013) identified 58 DEGs through microarray analysis of placentas from IVF, SCNT, and artificially inseminated cattle, showing enrichment in organ development; extracellular structure, matrix tissue, and the development, regulation, and maintenance of blood vessels and the vascular system. The molecular mechanisms underlying placental development and function are highly complex and involve many interconnected regulatory pathways. In the placenta of SCNT cattle, disruptions have been observed in extracellular matrix and adhesion, immune-related signaling pathways, and nutrient transport-related pathways (Ledgard et al., 2009). In our previous research, multi-omics analyses suggested that placental hypertrophy in SCNT cattle may be associated with abnormalities in urea and ion transmembrane transport signaling pathways (Gao et al., 2019). These disruptions in regulatory networks profoundly affect placental development and formation, potentially leading to fetal malformation or miscarriage. Excessive placental proliferation has emerged as a crucial factor contributing to the functional abnormalities observed in cloned placentas. In this study, transcriptome sequencing of SCNT and CON bovine placentas revealed that DEGs in SCNT placentas were predominantly enriched in energy metabolism, growth hormone signaling, cell differentiation, cell cycle-related signaling pathways, as well as the Hippo and PI3K-Akt signaling pathways. Among the DEGs, *Ccnd1* was identified as a key gene involved in both the Hippo and PI3K-Akt signaling pathways. The Hippo signaling pathway plays a vital role in tissue development, regeneration, and stem cell maintenance. Its core component, *Yap1*, regulates organ size, tissue regeneration, and cell proliferation (Yu et al., 2015). The biological functions of the Hippo signaling pathway closely overlap those of the TGF-β signaling pathway. In human placental tissues, Yap1 has been shown to specifically bind to Smad7, facilitating its recruitment to active TGFβRi and enhancing Smad7-mediated inhibition of Smad3/4 transcription (Mauviel et al., 2012). Research by Hiemer et al. (2014) demonstrated that the nuclear localization of Yap1 varies among breast cancer cell lines, influencing their sensitivity to TGF-β-induced growth arrest. The Wnt signaling pathway, which plays a central role in cell regulation, stem cell expansion, and regeneration, is closely linked to β-catenin as a key regulatory factor (Nusse & Clevers, 2017). Yap1 can directly bind to β-catenin, preventing its nuclear translocation and thereby inhibiting Wnt signaling (Azzolin et al., 2014). Deng et al. (2018) further confirmed that overexpression of Yap1 significantly increases the expression of Wnt/β-Catenin target genes *Lgr5* and *cyclinD1*. Additionally, Yap1 mediates the regulatory effects of both Wnt/β-catenin and insulin-like growth factor signaling on cardiomyocyte proliferation (Heallen et al., 2011). Despite these insights, studies specifically addressing the regulatory roles of YAP1 in the placentas of SCNT animals are limited.

In this study, PMSCs were isolated from both cloned and CON cattle. Cell proliferation assays demonstrated a significantly greater proliferative capacity in SCNT-derived bPMSCs compared to CON-derived bPMSCs, consistent with previous research (Miglino et al., 2007). In addition, YAP1 protein expression was significantly greater in SCNT blastocysts, placental tissues, and PMSCs compared to CON placental tissues, while phosphorylated YAP1 levels were markedly reduced in SCNT placental tissues and PMSCs. This reduction was associated with a significant increase in functional nuclear YAP1 protein in SCNT placental tissues. The Hippo signaling pathway is known to negatively regulate cell proliferation by inhibiting *Yap1*, thereby promoting cell differentiation and regulating organ size (Heallen et al., 2011; Zhang, 2015). Camargo et al. (2007) demonstrated that *Yap1*-specific overexpression in the mouse liver results in a greater than 4-fold increase in liver size, while termination of Yap1 overexpression restores the liver to normal size. Conversely, *Yap1* deficiency in the heart impedes cardiomyocyte proliferation, leading to incomplete cardiac development (Gong et al., 2021; Patel et al., 2017; von Gise et al., 2012; Weiler et al., 2017). Our findings suggest that overactivation of *Yap1* may be a key factor influencing placental hypertrophy in SCNT cattle. Previous studies have also shown that YAP1 can induce the cell cycle regulatory gene *Ccnd1*, linking YAP1 activation to abnormal cell cycle regulation. Down-regulation of *Yap1* has been shown to inhibit bladder cancer cell proliferation and induce cell cycle arrest in the G1 phase by reducing the expression of CCND1 and other G1 phase-related molecules. Notably, this arrest can be reversed by the up-regulation of *Yap1* expression (Mizuno et al., 2012; Wang et al., 2013; Wu et al., 2019). In this study, YAP1 overexpression in SCNT bPMSCs was accompanied by a significant reduction in phosphorylated YAP1 levels, while CCND1 exhibited a parallel increase in expression. Given the role of CCND1 in regulating cell proliferation and promoting G1/S cell cycle progression, SCNT bPMSCs demonstrated enhanced DNA synthesis, accelerated cell division, and rapid cell cycle progression. Furthermore, cyclin-dependent kinases and cell proliferation-related genes were expressed at significantly higher levels in SCNT bPMSCs compared to CON bPMSCs, indicating a markedly greater proliferative capacity.

To explore whether the enhanced proliferation of bPMSCs is attributable to the regulation of CCND1 by YAP1, these findings were validated using YAP1 overexpression and knockdown bPMSC models. Results confirmed that YAP1 plays a pivotal role in regulating bPMSC proliferation. Deletion of the YAP1 gene significantly reduced the proportion of S-phase cells, resulting in proliferation levels similar to those observed in CON bPMSCs. These findings suggest that YAP1 promotes SCNT bPMSC proliferation via the regulation of CCND1. Co-IP, luciferase, and ChIP interaction assays revealed that YAP1 binds to the proximal promoter of CCND1 (pCCND1-579-1) in SCNT bPMSCs, thereby promoting CCND1 expression. Additionally, CCND1 forms a complex with CDK6, facilitating G1-S cell cycle progression in SCNT bPMSCs. Within the cell, the activated CCND1-CDK4/CDK6 complex translocates to the nucleus and promotes the transcription of *E2F* transcription factors. These transcription factors regulate genes required for cell proliferation, driving cells into the S phase. The expression of CCND1 peaks in the late G1 phase, followed by its nuclear export during the S phase and subsequent ubiquitination and degradation (Chen et al., 2021; Wang et al., 2006; Zhong et al., 2010). Studies have demonstrated that reducing YAP1 or inhibiting its nuclear transport in breast cancer cells significantly reduces CDK6 expression and restores sensitivity to CDK4/6 inhibitors, thereby impacting the sensitivity of cancer cells to CDK4/6 inhibitors (Li et al., 2018b). In addition, the Hippo signaling pathway plays a crucial role in placental development by promoting cell proliferation and maintaining stemness (Meinhardt et al., 2020). However, its involvement in SCNT bovine placental hypertrophy has not been fully characterized. In this study, we demonstrated that YAP1 forms a complex

with CDK6 by binding to the *CCND1* proximal promoter (pCCND1-579-1) in SCNT placentas, driving G0/G1-S cell cycle progression in SCNT bPMSCs. These findings provide the first mechanistic insights into the role of the Hippo signaling pathway in controlling placental cell proliferation in SCNT animals, providing a foundation for understanding placental development in cloned cattle and advancing somatic cloning research.

CONCLUSIONS

This study revealed that the Hippo signaling pathway, specifically YAP1, regulates placental hyperplasia in cloned cattle by promoting CCND1-CDK6 expression and facilitating cell cycle progression. Understanding these molecular mechanisms has theoretical and practical implications, offering a potential avenue for enhancing cloning efficiency and advancing efforts in species conservation.

DATA AVAILABILITY

The datasets produced and/or analyzed in the current study are available from the corresponding author upon reasonable request. The raw RNA-seq data analyzed in this study are available from NCBI database (BioProjectID PRJNA1177607), China National Center for Bioinformation database of Genome Sequence Archive (GSA) (CRA014398), and Science Data Bank database (doi: 10.57760/sciencedb.j00139.00114).

SUPPLEMENTARY DATA

Supplementary data to this article can be found online

COMPETING INTERESTS

The author declare that they have no competing interests.

AUTHORS' CONTRIBUTIONS

G.H.S. and G.P.L. initiated and supervised the study; S.S.W. and X.Y.Z. performed most experiments and analyses; L.Y. and G.H.S. prepared the somatic cell nucleus transfer embryos; C.H. and D.W. performed RNA-seq experiments and data analysis; X.F.L., L.S.S., and C.L.B. provided instructive suggestions and revised the manuscript; S.S.W. and G.H.S. wrote the manuscript. All authors read and approved the final version of the manuscript.

ACKNOWLEDGMENTS

We utilized templates from BioRender software as the foundation for our figures.

REFERENCES

Aggarwal P, Vaites LP, Kim JK, et al. 2010. Nuclear cyclin D1/CDK4 kinase regulates *CUL4* expression and triggers neoplastic growth via activation of the PRMT5 methyltransferase. *Cancer Cell*, **18**(4): 329–340.

Arnold DR, Fortier AL, Lefebvre R, et al. 2008. Placental insufficiencies in cloned animals - A workshop report. *Placenta*, **29**(Suppl 1): 108–110.

Arnold DR, Gaspar RC, da Rocha CV, et al. 2017. Nuclear transfer alters placental gene expression and associated histone modifications of the placental-specific imprinted gene pleckstrin homology-like domain, family A, member 2 (*PHLDA2*) in cattle. *Reproduction, Fertility and Development*, **29**(3): 458–467.

Azzolin L, Panciera T, Soligo S, et al. 2014. YAP/TAZ incorporation in the β-catenin destruction complex orchestrates the Wnt response. *Cell*, **158**(1): 157–170.

Bajoria R, Sooranna SR, Ward BS, et al. 2002. Prospective function of placental leptin at maternal-fetal interface. *Placenta*, **23**(2-3): 103–115.

Biase FH, Rabel C, Guillomot M, et al. 2016. Massive dysregulation of genes involved in cell signaling and placental development in cloned cattle conceptus and maternal endometrium. *Proceedings of the National Academy of Sciences of the United States of America*, **113**(51): 14492–14501.

Boss AL, Chamley LW, James JL. 2018. Placental formation in early pregnancy: how is the centre of the placenta made?. *Human Reproduction Update*, **24**(6): 750–760.

Camargo FD, Gokhale S, Johnnidis JB, et al. 2007. YAP1 increases organ size and expands undifferentiated progenitor cells. *Current Biology*, **17**(23): 2054–2060.

Canel N, Bevacqua R, Fernández-Martín R, et al. 2010. Activation with ionomycin followed by dehydroleucodine and cytochalasin B for the production of parthenogenetic and cloned bovine embryos. *Cellular Reprogramming*, **12**(4): 491–499.

Chae JI, Cho SK, Seo JW, et al. 2006. Proteomic analysis of the extraembryonic tissue from cloned porcine embryos. *Molecular & Cellular Proteomics*, **5**(9): 1559–1566.

Chavatte-Palmer P, de Sousa N, Laigre P, et al. 2006. Ultrasound fetal measurements and pregnancy associated glycoprotein secretion in early pregnancy in cattle recipients carrying somatic clones. *Theriogenology*, **66**(4): 829–840.

Chen ZG, Xie YY, Luo HC, et al. 2021. NAP1L1 promotes proliferation and chemoresistance in glioma by inducing CCND1/CDK4/CDK6 expression through its interaction with HDGF and activation of c-Jun. *Aging*, **13**(24): 26180–26200.

Cheraghi S, Razi M, Malekinejad H. 2015. Involvement of cyclin D1 and E2f1 in zearalenone-induced DNA damage in testis of rats. *Toxicon*, **106**: 108–116.

Constant F, Guillomot M, Heyman Y, et al. 2006. Large offspring or large placenta syndrome? Morphometric analysis of late gestation bovine placentomes from somatic nuclear transfer pregnancies complicated by hydrallantois. *Biology of Reproduction*, **75**(1): 122–130.

Deng FH, Peng L, Li ZJ, et al. 2018. YAP triggers the Wnt/β-catenin signaling pathway and promotes enterocyte self-renewal, regeneration and tumorigenesis after DSS-induced injury. *Cell Death & Disease*, **9**(2): 153.

Dong JX, Feldmann G, Huang JB, et al. 2007. Elucidation of a universal size-control mechanism in *Drosophila* and mammals. *Cell*, **130**(6): 1120–1133.

Everts RE, Chavatte-Palmer P, Razzak A, et al. 2008. Aberrant gene expression patterns in placentomes are associated with phenotypically normal and abnormal cattle cloned by somatic cell nuclear transfer. *Physiological Genomics*, **33**(1): 65–77.

Fletcher CJ, Roberts CT, Hartwich KM, et al. 2007. Somatic cell nuclear transfer in the sheep induces placental defects that likely precede fetal demise. *Reproduction*, **133**(1): 243–255.

Gao GQ, Wang SY, Zhang JQ, et al. 2019. Transcriptome-wide analysis of the SCNT bovine abnormal placenta during mid- to late gestation. *Scientific Reports*, **9**(1): 20035.

Gong R, Jiang ZK, Zagidullin N, et al. 2021. Regulation of cardiomyocyte fate plasticity: a key strategy for cardiac regeneration. *Signal Transduction and Targeted Therapy*, **6**(1): 31.

Gorczyca G, Wartalski K, Romek M, et al. 2022. The molecular quality and mitochondrial activity of porcine cumulus-oocyte complexes are affected by their exposure to three endocrine-active compounds under 3D In vitro maturation conditions. *International Journal of Molecular Sciences*, **23**(9): 4572.

Gorczyca G, Wartalski K, Wiater J, et al. 2021. Anabolic steroids-driven regulation of porcine ovarian putative stem cells favors the onset of their neoplastic transformation. *International Journal of Molecular Sciences*, **22**(21): 11800.

Heallen T, Zhang M, Wang J, et al. 2011. Hippo pathway inhibits wnt signaling to restrain cardiomyocyte proliferation and heart size. *Science*,

332(6028): 458–461.

Hiemer SE, Szymaniak AD, Varelas X. 2014. The transcriptional regulators TAZ and YAP direct transforming growth factor β-induced tumorigenic phenotypes in breast cancer cells. *Journal of Biological Chemistry*, **289**(19): 13461–13474.

Hill JR. 2014. Incidence of abnormal offspring from cloning and other assisted reproductive technologies. *Annual Review of Animal Biosciences*, **2**: 307–321.

Hill JR, Burghardt RC, Jones K, et al. 2000. Evidence for placental abnormality as the major cause of mortality in first-trimester somatic cell cloned bovine fetuses. *Biology of Reproduction*, **63**(6): 1787–1794.

Huang YM, Zhang JC, Li XM, et al. 2023. Chromatin accessibility memory of donor cells disrupts bovine somatic cell nuclear transfer blastocysts development. *The FASEB Journal*, **37**(9): e23111.

Hwang JY, Oh JN, Park CH, et al. 2015. Dosage compensation of X-chromosome inactivation center-linked genes in porcine preimplantation embryos: non-chromosome-wide initiation of X-chromosome inactivation in blastocysts. *Mechanisms of Development*, **138**: 246–255.

Inoue K, Kohda T, Lee J, et al. 2002. Faithful expression of imprinted genes in cloned mice. *Science*, **295**(5553): 297–297.

Jiao F, Yan JB, Yang XY, et al. 2007. Effect of oocyte mitochondrial DNA haplotype on bovine somatic cell nuclear transfer efficiency. *Molecular Reproduction and Development*, **74**(10): 1278–1286.

Lankford L, Chen YJ, Saenz Z, et al. 2017. Manufacture and preparation of human placenta-derived mesenchymal stromal cells for local tissue delivery. *Cytotherapy*, **19**(6): 680–688.

Ledgard A, Lee RSF, Couldrey C, et al. 2009. Dickkopf-1 expression during early bovine placentation and its down-regulation in somatic cell nuclear transfer (SCNT) pregnancies. *Journal of Reproduction and Development*, **55**(5): 467–474.

Lee RSF, Peterson AJ, Donnison MJ, et al. 2004. Cloned cattle fetuses with the same nuclear genetics are more variable than contemporary half-siblings resulting from artificial insemination and exhibit fetal and placental growth deregulation even in the first trimester. *Biology of Reproduction*, **70**(1): 1–11.

Lee SY, Park JY, Choi YJ, et al. 2007. Comparative proteomic analysis associated with term placental insufficiency in cloned pig. *Proteomics*, **7**(8): 1303–1315.

Li NN, Zeng J, Sun FZ, et al. 2018a. *p27* inhibits CDK6/CCND1 complex formation resulting in cell cycle arrest and inhibition of cell proliferation. *Cell Cycle*, **17**(19-20): 2335–2348.

Li ZQ, Razavi P, Li Q, et al. 2018b. Loss of the FAT1 tumor suppressor promotes resistance to CDK4/6 inhibitors via the hippo pathway. *Cancer Cell*, **34**(6): 893–905. e8.

Liu Y, Shi HR, Wu D, et al. 2021. The protective benefit of heme oxygenase-1 gene-modified human placenta-derived mesenchymal stem cells in a N-nitro-L-arginine methyl ester-induced preeclampsia-like rat model: possible implications for placental angiogenesis. *Stem Cells and Development*, **30**(19): 991–1002.

Magatti M, Stefani FR, Papait A, et al. 2019. Perinatal mesenchymal stromal cells and their possible contribution to fetal-maternal tolerance. *Cells*, **8**(11): 1401.

Malin K, Witkowska-Piłaszewicz O, Papis K. 2022. The many problems of somatic cell nuclear transfer in reproductive cloning of mammals. *Theriogenology*, **189**: 246–254.

Matoba S, Zhang Y. 2018. Somatic cell nuclear transfer reprogramming: mechanisms and applications. *Cell Stem Cell*, **23**(4): 471–485.

Mauviel A, Nallet-Staub F, Varelas X. 2012. Integrating developmental signals: a Hippo in the (path)way. *Oncogene*, **31**(14): 1743–1756.

Meinhardt G, Haider S, Kunihs V, et al. 2020. Pivotal role of the transcriptional co-activator YAP in trophoblast stemness of the developing human placenta. *Proceedings of the National Academy of Sciences of the United States of America*, **117**(24): 13562–13570.

Miglino MA, Pereira FTV, Visintin JA, et al. 2007. Placentation in cloned cattle: structure and microvascular architecture. *Theriogenology*, **68**(4): 604–617.

Min B, Cho S, Park JS, et al. 2015. Transcriptomic features of bovine blastocysts derived by somatic cell nuclear transfer. *G3 Genes| Genomes| Genetics*, **5**(12): 2527–2538.

Mizuno T, Murakami H, Fujii M, et al. 2012. YAP induces malignant mesothelioma cell proliferation by upregulating transcription of cell cycle-promoting genes. *Oncogene*, **31**(49): 5117–5122.

Moon S, Park SY, Park HW. 2018. Regulation of the Hippo pathway in cancer biology. *Cellular and Molecular Life Sciences*, **75**(13): 2303–2319.

Nusse R, Clevers H. 2017. Wnt/β-Catenin signaling, disease, and emerging therapeutic modalities. *Cell*, **169**(6): 985–999.

Oback B. 2008. Climbing mount efficiency-small steps, not giant leaps towards higher cloning success in farm animals. *Reproduction in Domestic Animals*, **43**(S2): 407–416.

Ogura A, Inoue K, Wakayama T. 2013. Recent advancements in cloning by somatic cell nuclear transfer. *Philosophical Transactions of the Royal Society B: Biological Sciences*, **368**(1609): 20110329.

Ogura A, Matoba S, Inoue K. 2021. 25th ANNIVERSARY OF CLONING BY SOMATIC-CELL NUCLEAR TRANSFER: epigenetic abnormalities associated with somatic cell nuclear transfer. *Reproduction*, **162**(1): F45–F58.

Park JY, Kim JH, Choi YJ, et al. 2009. Comparative proteomic analysis of malformed umbilical cords from somatic cell nuclear transfer-derived piglets: implications for early postnatal death. *BMC Genomics*, **10**: 511.

Patel SH, Camargo FD, Yimlamai D. 2017. Hippo signaling in the liver regulates organ size, cell fate, and carcinogenesis. *Gastroenterology*, **152**(3): 533–545.

Peter AT. 2013. Bovine placenta: a review on morphology, components, and defects from terminology and clinical perspectives. *Theriogenology*, **80**(7): 693–705.

Pool M, Leuvenink H, Moers C. 2019. Reparative and regenerative effects of mesenchymal stromal cells-promising potential for kidney transplantation?. *International Journal of Molecular Sciences*, **20**(18): 4614.

Ravelich SR, Shelling AN, Wells DN, et al. 2006. Expression of TGF-β1, TGF-β2, TGF-β3 and the receptors TGF-βRI and TGF-βRII in placentomes of artificially inseminated and nuclear transfer derived bovine pregnancies. *Placenta*, **27**(2-3): 307–316.

Rivera RM. 2021. 209 Large offspring syndrome: effects of in vitro production on embryo epigenetics and development. *Journal of Animal Science*, **99**(S1): 114–115.

Ross PJ, Rodriguez RM, Iager AE, et al. 2009. Activation of bovine somatic cell nuclear transfer embryos by PLCZ cRNA injection. *Reproduction*, **137**(3): 427–437.

Salilew-Wondim D, Tesfaye D, Hossain M, et al. 2013. Aberrant placenta gene expression pattern in bovine pregnancies established after transfer of cloned or in vitro produced embryos. *Physiological Genomics*, **45**(1): 28–46.

Samiec M. 2022. Molecular mechanism and application of somatic cell cloning in mammals-past, present and future. *International Journal of Molecular Sciences*, **23**(22): 13786.

Samiec M, Skrzyszowska M. 2005. Molecular conditions of the cell nucleus remodelling/reprogramming process and nuclear-transferred embryo development in the intraooplasmic karyoplast injection technique: a review. *Czech Journal of Animal Science*, **50**(5): 185–195.

Samiec M, Skrzyszowska M. 2010. Preimplantation developmental capability of cloned pig embryos derived from different types of nuclear donor somatic cells. *Annals of Animal Science*, **10**(4): 385–398.

Sangalli JR, Sampaio RV, De Bem THC, et al. 2023. Cattle cloning by

somatic cell nuclear transfer. *In*: Moura MT. Somatic Cell Nuclear Transfer Technology. New York: Humana, 225–244.

Skrzyszowska M, Samiec M, Słomski R, et al. 2008. Development of porcine transgenic nuclear-transferred embryos derived from fibroblast cells transfected by the novel technique of nucleofection or standard lipofection. *Theriogenology*, **70**(2): 248–259.

Srirattana K, Kaneda M, Parnpai R. 2022. Strategies to improve the efficiency of somatic cell nuclear transfer. *International Journal of Molecular Sciences*, **23**(4): 1969.

Su GH, Wang LN, Gao GQ, et al. 2021a. C23 gene regulates the nucleolin structure and biosynthesis of ribosomes in bovine intraspecific and interspecific somatic cell nuclear transfer embryos. *The FASEB Journal*, **35**(11): e21993.

Su GH, Wu SS, Wu ML, et al. 2021b. Melatonin improves the quality of frozen bull semen and influences gene expression related to embryo genome activation. *Theriogenology*, **176**: 54–62.

Su XH, Gao GQ, Wang SY, et al. 2019. CircRNA expression profile of bovine placentas in late gestation with aberrant SCNT fetus. *Journal of Clinical Laboratory Analysis*, **33**(6): e22918.

Svarcova O, Laurincik J, Avery B, et al. 2007. Nucleolar development and allocation of key nucleolar proteins require de novo transcription in bovine embryos. *Molecular Reproduction and Development*, **74**(11): 1428–1435.

Tanaka S, Oda M, Toyoshima Y, et al. 2001. Placentomegaly in cloned mouse concepti caused by expansion of the spongiotrophoblast layer. *Biology of Reproduction*, **65**(6): 1813–1821.

Ticiani E, Rodrigues VHV, Willhelm BR, et al. 2020. Evidence of metabolic compartmentation in the bovine placenta and significance for the regulation of placental function and fetal growth in pregnancies bearing *in vivo*-or *in vitro*-produced embryos. *Livestock Science*, **236**: 104024.

Tsunoda Y, Kato Y. 2002. Recent progress and problems in animal cloning. *Differentiation*, **69**(4-5): 158–161.

Vajta G. 2007. Somatic cell nuclear transfer in its first and second decades: successes, setbacks, paradoxes and perspectives. *Reproductive Biomedicine Online*, **15**(5): 582–590.

von Gise A, Lin ZQ, Schlegelmilch K, et al. 2012. YAP1, the nuclear target of Hippo signaling, stimulates heart growth through cardiomyocyte proliferation but not hypertrophy. *Proceedings of the National Academy of Sciences of the United States of America*, **109**(7): 2394–2399.

Wakisaka-Saito N, Kohda T, Inoue K, et al. 2006. Chorioallantoic placenta defects in cloned mice. *Biochemical and Biophysical Research Communications*, **349**(1): 106–114.

Wang CG, Li ZP, Lu YN, et al. 2006. Cyclin D1 repression of nuclear respiratory factor 1 integrates nuclear DNA synthesis and mitochondrial function. *Proceedings of the National Academy of Sciences of the United States of America*, **103**(31): 11567–11572.

Wang LY, Li ZK, Wang LB, et al. 2020. Overcoming intrinsic H3K27me3 imprinting barriers improves post-implantation development after somatic cell nuclear transfer. *Cell Stem Cell*, **27**(2): 315–325. e5.

Wang Y, Xie CY, Li QC, et al. 2013. Clinical and prognostic significance of Yes-associated protein in colorectal cancer. *Tumor Biology*, **34**(4): 2169–2174.

Watanabe S, Nagai T. 2011. Survival of embryos and calves derived from somatic cell nuclear transfer in cattle: a nationwide survey in Japan. *Animal Science Journal*, **82**(2): 360–365.

Weiler SME, Pinna F, Wolf T, et al. 2017. Induction of chromosome instability by activation of yes-associated protein and forkhead box M1 in liver cancer. *Gastroenterology*, **152**(8): 2037–2051. e22.

Whitworth KM, Prather RS. 2010. Somatic cell nuclear transfer efficiency: how can it be improved through nuclear remodeling and reprogramming?. *Molecular Reproduction and Development*, **77**(12): 1001–1015.

Wu D, Liu Y, Liu XX, et al. 2020. Heme oxygenase-1 gene modified human placental mesenchymal stem cells promote placental angiogenesis and spiral artery remodeling by improving the balance of angiogenic factors *in vitro*. *Placenta*, **99**: 70–77.

Wu YJ, Zheng QQ, Li Y, et al. 2019. Metformin targets a YAP1-TEAD4 complex via AMPKα to regulate CCNE1/2 in bladder cancer cells. *Journal of Experimental & Clinical Cancer Research*, **38**(1): 376.

Yan ZH, Zhou YY, Fu J, et al. 2010. Donor-host mitochondrial compatibility improves efficiency of bovine somatic cell nuclear transfer. *BMC Developmental Biology*, **10**: 31.

Yang XZ, Smith SL, Tian XC, et al. 2007. Nuclear reprogramming of cloned embryos and its implications for therapeutic cloning. *Nature Genetics*, **39**(3): 295–302.

Young LE, Sinclair KD, Wilmut I. 1998. Large offspring syndrome in cattle and sheep. *Reviews of Reproduction*, **3**(3): 155–163.

Yu FX, Zhao B, Guan KL. 2015. Hippo pathway in organ size control, tissue homeostasis, and cancer. *Cell*, **163**(4): 811–828.

Zhang L. 2015. Control of growth and beyond: a special issue on Hippo signaling. *Acta Biochimica et Biophysica Sinica*, **47**(1): 1.

Zhong ZJ, Yeow WS, Zou CH, et al. 2010. Cyclin D1/cyclin-dependent kinase 4 interacts with filamin a and affects the migration and invasion potential of breast cancer cells. *Cancer Research*, **70**(5): 2105–2114.

Zhou C, Zhang JC, Zhang M, et al. 2020. Transcriptional memory inherited from donor cells is a developmental defect of bovine cloned embryos. *The FASEB Journal*, **34**(1): 1637–1651.